The evolution of the mass-size relation for early-type galaxies from z ∼1 to the present: dependence on environment, mass range and detailed morphology

Marc Huertas-Company, S. Mei, F. Shankar, Lauriane Delaye, A. Raichoor, G. Covone, A. Finoguenov, J. P. Kneib, O. Le Fevre, M. Povic

HAL Id: hal-01439479

https://hal.science/hal-01439479

Submitted on 21 May 2019

The evolution of the mass–size relation for early-type galaxies from $z \sim 1$ to the present: dependence on environment, mass range and detailed morphology

M. Huertas-Company,[1,2]★ S. Mei,[1,2] F. Shankar,[1] L. Delaye,[1,3] A. Raichoor,[4] G. Covone,[5,6] A. Finoguenov,[7] J. P. Kneib,[8] O. Le Fèvre[8] and M. Povič[9]

[1]*GEPI, Paris Observatory, 77 Avenue Denfert Rochereau, F-75014 Paris, France*
[2]*University Denis Diderot, 4 Rue Thomas Mann, F-75205 Paris, France*
[3]*CEA, IRFU, SAp, F-91191 Gif-sur-Yvette, France*
[4]*INAF – Osservatorio Astronomico di Brera, via Brera 28, I-20121 Milan, Italy*
[5]*Dipartimento di Scienze Fisiche, Università di Napoli 'Federico II', Via Cinthia, I-80126 Napoli, Italy*
[6]*INFN Sez. di Napoli, Compl. Univ. Monte S. Angelo, Via Cinthia, I-80126 Napoli, Italy*
[7]*Department of Physics, University of Helsinki, Gustaf Hällströmin katu2a, FI-00014 Helsinki, Finland*
[8]*Laboratoire d'Astrophysique de Marseille, CNRS-Université, Pôle de l'Étoile Site de Château-Gombert 38, rue Frédéric Joliot-Curie, F-13388 Marseille Cedex 13, France*
[9]*Instituto de astrofísica de Andalucía(IAA-CSIC), C/ Glorieta de la Astronomía s/n, E-18008 Granada, Spain*

ABSTRACT

We study the dependence of the galaxy size evolution on morphology, stellar mass and large-scale environment for a sample of 298 group and 384 field quiescent early-type galaxies from the COSMOS survey, selected from $z \sim 1$ to the present, and with masses $\log(M/M_\odot) > 10.5$.

From a detailed morphological analysis we infer that $\sim$80 per cent of passive galaxies with mass $\log(M/M_\odot) > 10.5$ have an early-type morphology and that this fraction does not evolve over the last 6 Gyr. However, the relative abundance of lenticular and elliptical galaxies depends on stellar mass. Elliptical galaxies dominate only at the very high mass end – $\log(M/M_\odot) > 11$ – while S0 galaxies dominate at lower stellar masses – $10.5 < \log(M/M_\odot) < 11$.

The galaxy size growth depends on galaxy mass range and early-type galaxy morphology, e.g. elliptical galaxies evolve differently than lenticular galaxies. At the low-mass end – $10.5 < \log(M/M_\odot) < 11$ – ellipticals do not show strong size growth from $z \sim 1$ to the present (10 to 30 per cent depending on the morphological classification). On the other end, massive ellipticals – $\log(M/M_\odot) > 11.2$ – approximately doubled their size. Interestingly, lenticular galaxies display different behaviour: they appear more compact on average and they do show a size growth of $\sim$60 per cent since $z = 1$ independent of stellar mass range.

We compare our results with state-of-the art semi-analytic models. While major and minor mergers can account for most of the galaxy size growth, we find that with present data and the theoretical uncertainties in the modelling we cannot state clear evidence favouring either merger or mass-loss via quasar and/or stellar winds as the primary mechanism driving the evolution.

The galaxy mass–size relation and size growth do not depend on environment in the halo mass range explored in this work (field to group mass $\log(M_h/M_\odot) < 14$), i.e. group and field galaxies follow the same trends. At low redshift, where we examine both Sloan Digital Sky Survey and COSMOS groups, this result is at variance with predictions from some current hierarchical models that show a clear dependence of size growth on halo mass for massive ellipticals ($\log(M_*/M_\odot) > 11.2$). In future work, we will analyse in detail if this result is specific of the observations and model used in this work.

★ E-mail: marc.huertas@obspm.fr

Brightest Cluster Galaxies (BCG) and satellite galaxies lie on the same mass–size relation, at variance with predictions from hierarchical models, which predict that BCGs should have larger sizes than satellites because they experience more mergers in groups over the halo mass range probed.

Key words: galaxies: elliptical and lenticular, cD – galaxies: evolution.

1 INTRODUCTION

The fact that massive quiescent galaxies experienced a strong size evolution in the last 10 Gyr is now a commonly accepted picture since first works on this topic were published (Daddi et al. 2005; Trujillo et al. 2006). Many independent groups using different data sets and selections have come up with similar conclusions, i.e. massive galaxies roughly doubled their size from $z \sim 1$ and probably increased it by $3-5$ from $z \sim 2$ (e.g. Buitrago et al. 2008; van der Wel et al. 2008; van Dokkum et al. 2008; Damjanov et al. 2011; Cimatti, Nipoti & Cassata 2012) even though there might be a population with larger sizes already in place at high redshift (e.g. Mancini et al. 2010; Saracco, Longhetti & Gargiulo 2011). As several works pointed out since the first publications came out, the result could be biased by a wrong estimate of stellar masses [which is usually done through spectral energy distribution (SED) fitting; e.g. Raichoor et al. 2011] and/or an underestimate of galaxy sizes at very high redshifts since surface brightness dimming could cause the loss of the very outer parts of galaxies (e.g. Bezanson et al. 2009; Hopkins et al. 2009). Independent measurements based on dynamical masses have however confirmed the compactness of several objects (e.g. Martinez-Manso et al. 2011; van de Sande et al. 2011; Newman et al. 2012) and it now seems clear that there is indeed a population of compact objects at high redshift. Some works also pointed out that we cannot exclude that the current galaxy selections might be biased and we are missing those compact objects in the nearby Universe, or selecting the most compact objects at high redshift (Valentinuzzi et al. 2010). This would be at variance with the work of Trujillo et al. (2009) that showed that there is not a strong evidence for a significant fraction of compact objects in the local Universe.

From the theoretical point of view, two main mechanisms have been proposed to increase galaxy size. Fan et al. (2008) proposed active galactic nuclei and supernovae feedback as the main responsible of galaxy expansion while Hopkins et al. (2006) and Naab, Johansson & Ostriker (2009) argued that minor dry mergers are the most efficient way to grow sizes since they affect the outer parts of the galaxy without significantly modifying the stellar mass nor the star formation (see also Shankar et al. 2011).

Several recent observational works have tried to disentangle the two scenarios. As a result, minor dry merging seems to emerge as the most plausible explanation for the size evolution (e.g. Trujillo, Ferreras & de La Rosa 2011) at least from $z \sim 1$, leading to an inside-out growth of galaxies (e.g. Tiret et al. 2011; Patel et al. 2012) even though there is still some debate. Newman et al. (2012) showed by carefully counting small companions in very deep images from the CANDELS survey (Grogin et al. 2011; Koekemoer et al. 2011) that minor mergers are roughly enough to account for the size evolution from $z \sim 1$ (provided that a short merger time-scale is assumed) and a combination of minor merging and star formation quenching can explain the galaxy growth from $z \sim 2$. Using morphological merging indicators, Bluck et al. (2011) reached at a similar conclusion and even argue that the problem is close to be solved [see also McLure et al. (2012) for similar considerations]. On

the other hand, López-Sanjuan et al. (2011, 2012) point out that for galaxies with masses $\log(M/M_\odot) > 11$ minor mergers are not the only process responsible for size growth since $z \sim 1$. These authors propose a scenario for which minor and major mergers contribute to ~ 55 per cent, while the remaining ~ 45 per cent to ~ 25 per cent is due to other processes and specially to younger galaxies (hence larger) arriving at later epochs (progenitor bias).

When measuring the galaxy mass–size relation and mass growth, different works use different sample selections though and this might lead to different conclusions. It is very rare in fact to find two works dealing with size evolution which apply the same criteria to select their galaxy sample and the same methodology to analyse the data. Some are based on star formation only (Papovich et al. 2012) whereas others on morphology (Cooper et al. 2012; Raichoor et al. 2012) or on a combination of both (e.g. van der Wel et al. 2008; Damjanov et al. 2011). Finally, many works combine a stellar mass selection with a quiescence criterion (e.g. van Dokkum et al. 2008; Newman et al. 2012) and generally the mass cuts are not always the same. See Damjanov et al. (2011) and Cimatti et al. (2012) for two different compilations of recent results. These different selections are based on the general idea that almost all massive galaxies are passive and have an early-type morphology, which is not always true as shown in recent works (e.g. van Dokkum et al. 2011; Trujillo, Carrasco & Ferré-Mateu 2012).

Another recent point of discussion in the literature is the role of environment. Recent observational studies show controversial results. Raichoor et al. (2012) studied the mass–size relation for morphologically selected early-type galaxies (ETGs) at $z \sim 1.2$ in three different environments (field, cluster and groups) and find that, on average, for masses $10 < \log(M/M_\odot) < 11.5$ cluster galaxies appear to be smaller at fixed stellar mass than field galaxies. Interestingly, in the same stellar mass range but at lower redshift, Cooper et al. (2012) find exactly the opposite trend using DEEP3 (Cooper et al. 2011). Larger sizes in the cluster environment are also observed at $z = 1.62$ by Papovich et al. (2012) with CANDELS data for passive galaxies with stellar masses larger than $\log(M/M_\odot) \sim 10.5$. However, other two works (Maltby et al. 2010; Rettura et al. 2010) do not find any trend with environment at $z < 0.4$ and ~ 1.2, respectively. The differences between these works are somehow puzzling but might come from the different sample selections (e.g. based on colour or Sérsic index versus visual morphology classification) and/or the way environment is measured (local versus global) and/or low statistics (high-redshift results indeed rely on some tens of galaxies).

We will address here these questions by carefully selecting a statistically significant sample of galaxies from the recently published COSMOS X-ray detected group galaxy sample (Finoguenov et al. 2007; George et al. 2011) as compared to the field. Within this sample we will dissect the properties of passive galaxies and look at the effects on the size growth of the galaxies with different morphology in different environments.

The paper is organized as follows: in Section 2, we describe the data sets used in this work and the derived quantities (morphologies, sizes and stellar masses) and in sections 3 and 4 we present

and discuss our main results. Throughout the paper, we consider a standard Λ cold dark matter cosmology ($\Omega_M = 0.3$, $\Omega_\Lambda = 0.7$).

2 DATA AND ANALYSIS

2.1 Data sets

We use two samples of galaxies from the COSMOS survey belonging to two different environments: groups and field.

The group sample is composed of groups in the COSMOS field that have been detected as extended X-ray emitters (Finoguenov et al. 2007), which is a strong signature of virialized structures, and have several spectroscopic confirmed members. The full sample contains groups with halo masses from $M_{200C}/M_\odot \sim 10^{13}$ to $\sim 10^{14}$ as measured by weak lensing (Leauthaud et al. 2010) and spans the redshift range $0.2 < z < 1.0$. Group members have been selected based on photometric redshifts (and spectroscopic redshifts when available) derived from the extensive COSMOS multiwavelength imaging (Ilbert et al. 2009). For this work, we use two group samples, for which details on the galaxy selection can be found in George et al. (2011) who carried out a careful analysis of potential biases and contaminations.

(i) We call the first sample *central* which includes only galaxies within $0.5R_{200C}$ and a probability of being a group member greater than 0.5. We then expect a contamination of ~ 15 per cent and a completeness of ~ 90 per cent (George et al. 2011).

(ii) The second *larger* sample includes galaxies within R_{200C} and is mainly used to increase statistics, using always the central sample to control contamination effects if environment is discussed. For the larger selection, the contamination is ~ 30 per cent and the completeness ~ 90 per cent (George et al. 2011).

To both samples, we apply a magnitude cut $I814(AB) < 24$ mag required for size estimates and morphology classification as explained in Sections 2.2 and 2.3.

Field galaxies are selected in the COSMOS field in the same redshift range as group members and with the same magnitude cut but making sure that they do not belong to any detected group [e.g. with GROUP$_{ID} = -1$ in the George et al. (2011) group catalogue]. We assume that these galaxies lie in a dark matter (DM) halo of mass $M_{200C}/M_\odot < 10^{13.2}$, otherwise they should have been detected as groups members – see fig. 1 from George et al. (2011). The field sample contains 3760 galaxies.

2.2 Sizes and masses

Sizes of all galaxies have been estimated on the COSMOS *Hubble Space Telescope (HST)*/ACS F814W images (MOSAIC v2.0; Koekemoer et al. 2007) using GALAPAGOS (Barden et al. 2012) which is an IDL-based pipeline to run SEXTRACTOR (Bertin & Arnouts 1996) and GALFIT (Peng et al. 2002) together. We basically fit every galaxy in the field and in the group sample with a 2D Sérsic profile (Sersic 1968) using the default GALAPAGOS parameters as described and tested in Häussler et al. (2007). Our number of failures (i.e. fits that do not converge) is less than 5 per cent. The point spread function (PSF) used for the fitting is taken from Rhodes et al. (2007) who computed spatially varying model PSFs for the COSMOS survey taking into account variations in the effective *HST* focus positions. For this work, we used a single PSF [estimated at the average focus position for the COSMOS survey ($\Delta = -2\,\mu m$)] for all the galaxies after checking that it does not introduce significant biases (see below).

The reliability of our size estimates is estimated by placing mock galaxies ($1 < n < 8$, $0.1 < r_e < 1.5$ arcsec, $17 < I < 24$ mag) in a real background. In our simulations, we also explore the possible biases due to local overdensities by dropping the mock galaxies in the same positions as in real high-redshift clusters. We also explore in the simulations the possible effects of a variable PSF by using a different PSF for simulating and for fitting. Both PSFs are taken from the Rhodes et al. (2007) PSFs models using the tabulation of the positional dependence of the PSF. We find that our size measurements are unbiased ($|\langle (r_{e,out} - r_{e,in})/r_{e,in}\rangle| < 0.1$) with a reasonable scatter ($\sqrt{Var[(r_{e,out} - r_{e,in})/r_{e,in}]} < 0.2$) up to $I_{814}(AB) < 24$ mag, $r_{e,in} < 1.0$ arcsec and $\mu_{814W} < 24$ mag $\times$ arcsec^{-2} (Fig. 1 and Delaye et al., in preparation). All galaxies in our sample have surface brightness brighter than $\mu_{814W} = 24$ mag $\times$ arcsec^{-2} so our size estimates are reliable according to the simulations.

Since we are using the same wavelength to estimate sizes up to $z \sim 1$, we estimate sizes in different rest frames at different redshifts (e.g. from the r-band rest frame at $z \sim 0.2$ to the B-band rest frame at $z \sim 1$). Recent work by Damjanov et al. (2011) and Cassata et al. (2011) has shown that sizes in the ultraviolet (UV) and optical rest frame strongly correlate, with sizes in the UV rest frame being only ~ 10 per cent smaller than those in the optical (see also Cimatti et al. 2012). Therefore, an additional (small) artificial size difference could be created when estimating the evolution between low- and high-redshift data. However, as shown in Section 3 and in Fig. 9, the size evolution we measure in our sample for ETGs is fully consistent with previous published results, specially with the ones of Newman et al. (2012) who computed sizes in a unique rest-frame optical filter. Therefore, we do not expect a significant bias due to this issue.

Throughout the paper, we will use circularized effective radii as primary size estimator, i.e. $r_e^{circ} = r_e^{fit} \times \sqrt{b/a}$.

Stellar masses are computed through SED fitting using the Bayesian code described in Bundy et al. (2006) (KB06) which employs Bruzual & Charlot (2003) (BC03) models with a Chabrier initial mass function (IMF), and published in George et al. (2011) catalogues. More details can be found in section 2.3 of Leauthaud et al. (2010).

2.3 Morphology

Galaxy morphologies in the group and field samples are also computed on the *HST*/ACS F814W images with GALSVM, a code for automated morphological classification based on support vector machines specially designed for high-redshift data (Huertas-Company et al. 2008, 2009). The code requires a visually classified training set which is used to simulate galaxies at higher redshift. The training set used in this work is a combination of the Nair & Abraham (2010) sample of $\sim 14\,000$ galaxies and the EFIGI project (Baillard et al. 2011) both from the Sloan Digital Sky Survey (SDSS) DR4. Our final training set therefore contains $\sim 20\,000$ galaxies.[1] We follow the Bayesian approach presented in Huertas-Company et al. (2011) to associate with every galaxy four probabilities of being in four morphological classes as defined in the local universe by Nair & Abraham (2010), i.e. ellipticals ($E0$, $E+$), lenticulars ($S0-$, $S0$, $S0+$, $S0/a$), early spirals (Sa, Sab, Sb, Sbc) or late spirals (Sc, Sd, Sdm, Sm, Im): $P(E)$, $P(S0)$, $P(Sab)$, $P(Scd)$. Errors in probabilities are computed by bootstrapping, i.e. we repeat the classification

---

[1] An updated and stable version of the code as well as the training set used for this work is available at http://gepicom04.obspm.fr/galSVM/Home.html
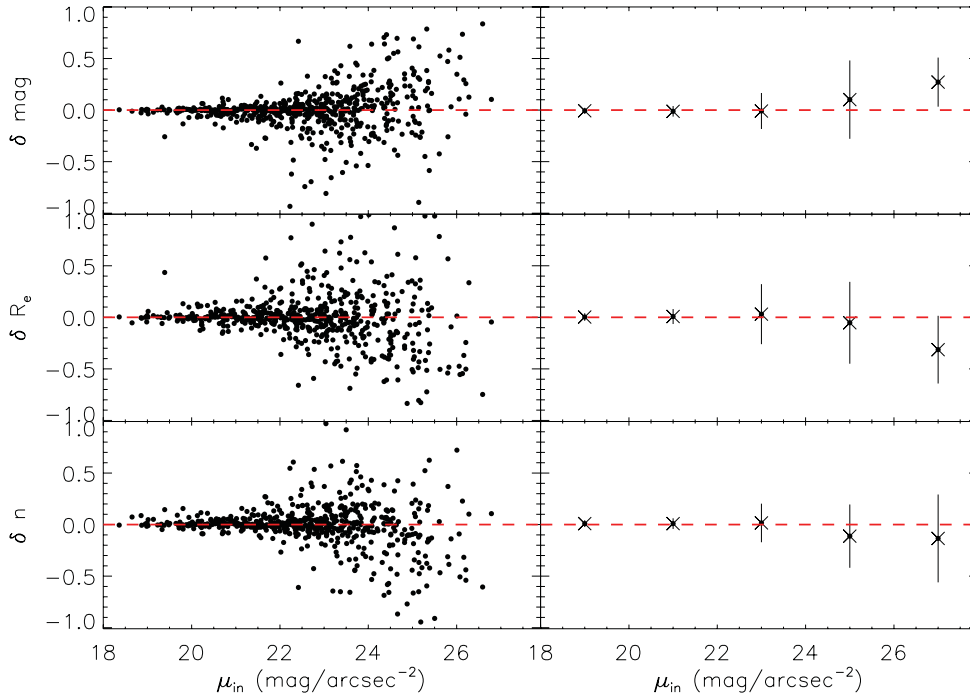
Figure 1. Results of simulations to assess the accuracy of our size estimates. Left-hand panels show the difference between the input and output magnitudes (top-left), effective radii (middle-left) and Sérsic index (bottom-left) for individual simulated galaxies as a function of surface brightness. Right-hand panels show the average bias and dispersions for different surface brightness bins.

10 times with randomly selected training sets from the main sample and keep the average probability for each galaxy as the final classification (see Huertas-Company et al. 2011 for more details). We then select as elliptical and lenticular galaxies the galaxies for which $max(P(E), P(S0), P(Sab), P(Scd)) = P(E)$ and $max(P(E), P(S0), P(Sab), P(Scd)) = P(S0)$, respectively. ETGs are then defined as the combination of both populations. With this selection, the completeness for ETGs is ∼95 per cent and the contamination rate is expected to be less than 7 per cent as stated by detailed comparisons with visual morphological classifications at $z \sim 1.3$ from Mei et al. (2009, 2012) in the Lynx super-cluster at $z = 1.26$. Our classification is therefore very close to a visual classification. This point is also confirmed by the fact that the axis ratio distribution of our early-type sample is very close to the one reported by Buitrago et al. (2011) from a visually classified sample (see Fig. 2 and their fig. 2).

To compare our morphological classification with those often used in the literature, we estimated the contamination that would suffer a selection of ETGs, based on a simple $n > 2.5$ cut. We find that such a sample would be contaminated by approximately 50 per cent of early spirals (see also Mei et al. 2012). We refer to Section 3 for a detailed analysis of the implications of such a selection.

Separating ellipticals from lenticulars is extremely challenging even by eye, so our classification is necessarily more contaminated. Simulations show that we are close to 30 per cent uncertainties, similar to those observed in other works (e.g. by visual morphological classifications by Postman et al. 2005). Our visually trained probabilistic approach for galaxy classification allows us to distinguish galaxies based on a quantitative separation in the parameter space that corresponds to that usually used to separate S0s and ellipticals in the local Universe (e.g. by visual classification). Indeed, the stel-

lar mass and axis ratio distributions of the two populations shown in Fig. 2 present different behaviours, as stated by Kuiper tests ($P < 0.6$), confirming that we are seeing separate populations and that the classification is not random. Ellipticals appear rounder, more massive on average, with slightly higher Sérsic indices and larger sizes. In order to double check our separation between lenticulars and ellipticals we performed two additional tests. First, we took the visually classified sample of Nair & Abraham (2010) in the SDSS, cross-correlated it with the Sérsic decompositions recently published by Simard et al. (2011) and looked at the same properties which we studied for our high-redshift sample. Results are shown in Fig. 3. We do clearly observe the same trends, i.e. lenticulars are also more elongated and slightly more compact than ellipticals, even though they are less pronounced than in the high-redshift sample. This test confirms that our E/S0 classification is consistent with the local visual classification, as expected. As a second step, two of us (MHC and SM) made visual classifications of our two automatically defined classes. We find that the two classifications of E/S0s agree at ∼80 per cent at $z < 0.5$ and ∼70 per cent at $z > 0.5$ which are fully consistent with the results from simulations and also with the differences found between independent human classifiers (e.g. Postman et al. 2005). However, in order to make sure that our results are not biased because of the automated method used, we double check our main results using visual classifications (see Appendix A) and comment in our analysis in subsequent sections whenever there is a significant difference.

We deduce that the population of elliptical galaxies selected through our method is dominated by pure bulge systems whereas an important fraction of what we call lenticulars have a disc component (but not observed arms) even if they are still bulge dominated. We also note that a simple Sérsic based selection of any kind would not allow the separation between these two populations.
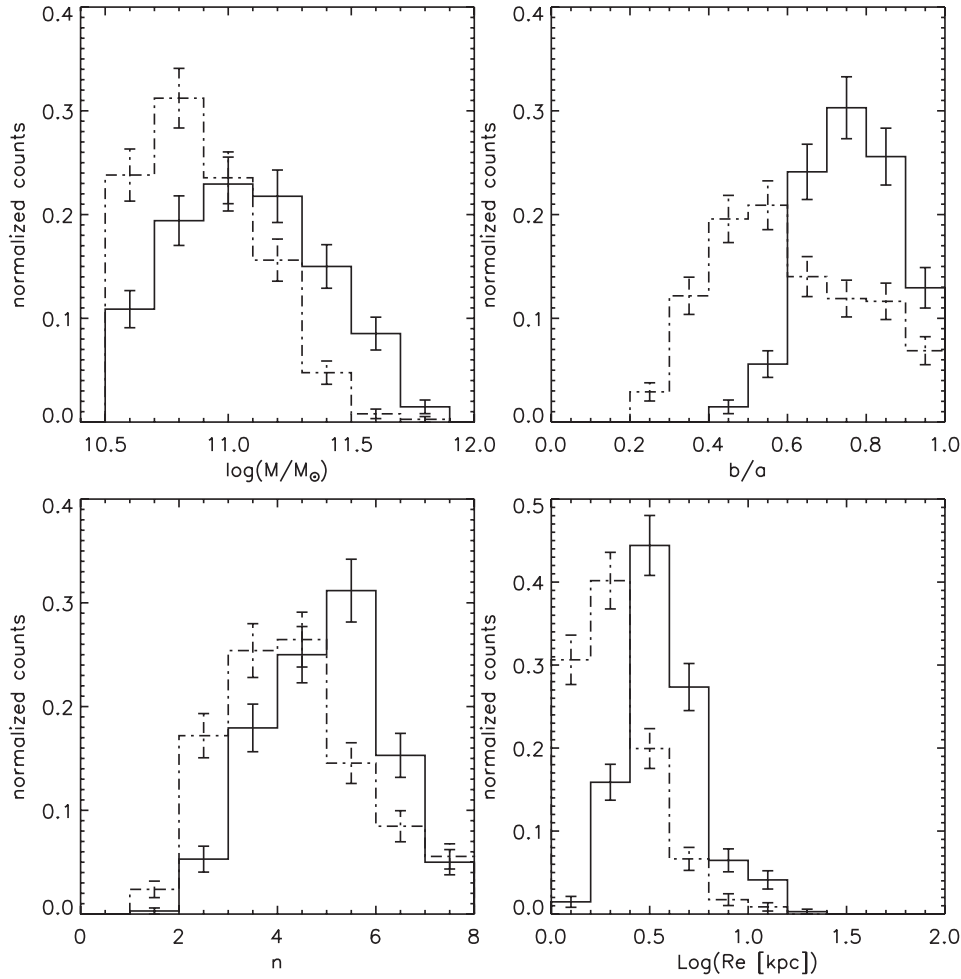
Figure 2. Stellar mass (top-left panel), axis ratio (top-right panel), Sérsic index (bottom-left panel) and size distributions (bottom-right panel) of morphologically classified ellipticals (solid line) and S0s (dashed line) with the automated procedure described in the text. Error bars are Poissonian. S0s and ellipticals have different parameter distributions, which prove that the algorithm indeed separates two different populations of galaxies and does it in a quantitative and re-producible way.

2.4 Completeness

Completeness of our sample is mainly driven by the apparent magnitude cut ($I_{814}(AB) < 24$ mag) required to properly estimate morphologies and sizes. Our main results in the following are shown as a function of stellar mass. Therefore, it is important to understand how this magnitude selection is translated in terms of stellar mass completeness to estimate how much the results might be affected by selection effects. Since in this work we focus on passive ETGs (see Section 3.1), all the completeness values are given for that population.

We used an approach similar to Pozzetti et al. (2010) and Giodini et al. (2012). For each passive galaxy we compute its limiting stellar mass ($M_*^{\lim}$) which is the stellar mass it would have if its apparent magnitude was equal to the limiting magnitude of the survey [$I_{814}(AB) = 24$ mag in our case]. This value is given by the relation $\log(M_*^{\lim}) = \log(M_*) - 0.4(I - I_{\lim})$ following Pozzetti et al. (2010). We compute this limiting mass for the 20 per cent faintest galaxies in each redshift bin and estimate the 95 per cent completeness as the 95th percentile of the resulting distribution. Following this approach, we obtain a 95 per cent completeness for galaxies with stellar masses greater than $\log(M_*/M_\odot) \sim 9.56$ at $z \sim 0.2$ and $\log(M_*/M_\odot) \sim 10.57$ at $z \sim 1$ (Fig. 4).

We note that the mass completeness for the COSMOS sample has been largely discussed in the literature (e.g. Meneux et al. 2009; Tasca et al. 2009; Pozzetti et al. 2010; Giodini et al. 2012) finding similar values.

In order to further check that low surface brightness objects are not lost, we carried a new set of simulations close to the ones performed to calibrate the size recovery. We modelled 2000 ETGs ($B/T > 0.6$) with effective radii varying from 0.1 to 1.5 arcsec and magnitudes at the faint end of the survey detection limit ($23 < I_{814} < 26$), dropped them in real background and computed the detection rate as a function of magnitude and size (Fig. 5). Galaxies with $I_{814} < 24$ of all sizes (and hence all surface brightness) are all detected thus confirming that our analysis sample is complete.

3 RESULTS

3.1 Sample selection

We investigate in this section how the sample selection affects the observed mass–size relation and size evolution of selected galaxies. We compare first three selections usually found in other works.
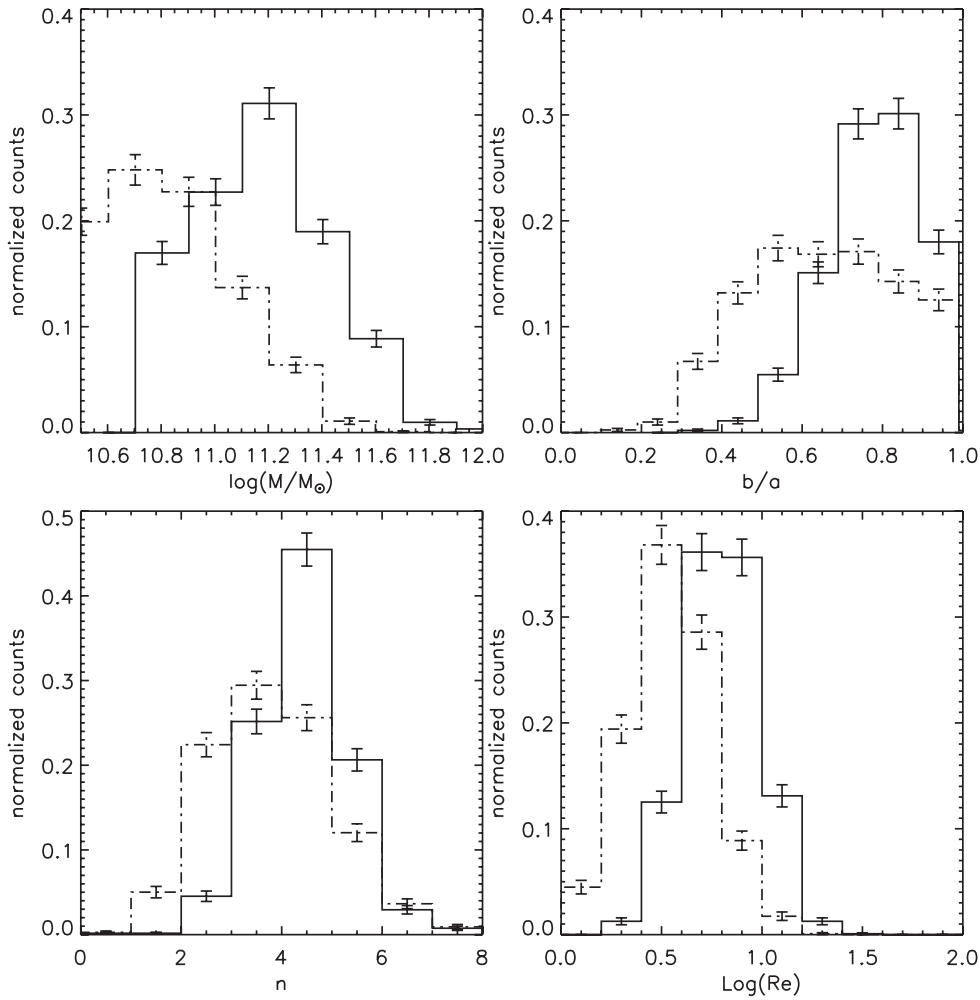
Figure 3. Same plot as Fig. 2 but for a local sample from the SDSS (Simard et al. 2011). The same trends as for the high-redshift sample are observed.

(i) *A passive selection*. This selection includes all quiescent galaxies with $\log(M/M_\odot) > 10.5$. The mass cut ensures that we are selecting a volume limited sample without being affected by incompleteness (see Section 2.4). Throughout this work, we will select quiescent or passive galaxies based on the $M(NUV) - M(R)$ dust corrected rest-frame colour as computed by Ilbert et al. (2009) by means of SED fitting. Ilbert et al. (2009) have shown that a $M(NUV) - M(R) > 3.5$ selection results in a good separation of passive and star-forming galaxies. See also Giodini et al. (2012) for a discussion on this selection on the same sample as the one used for this work.

(ii) *A Sérsic based selection*, i.e. we apply a simple $n > 2.5$ cut as usually done as well as the same stellar mass selection [$\log(M/M_\odot) > 10.5$].

(iii) *An ETG selection* in which we select all ETGs (ellipticals and lenticulars) with $\log(M/M_\odot) > 10.5$ from our morphological classification detailed in Section 2.3 independently of the star formation activity.

We show in Figs 6–8 the mass–size relations for samples (i), (ii) and (iii), respectively, in different environments and redshifts and we summarize the best-fitting parameters computed through a standard χ^2 minimization in Table 1. Also we show in the figures, with different symbols, the morphologies of the objects belonging to the given selection as well as the star formation activity (quiescent

or active) colour coded for selection (ii) and (iii). We also show the position of the brightest group galaxies (BGGs), defined as the most massive galaxies within an NFW scale radius of the X-ray position, from the George et al. (2011) catalogue. Note that some of them are morphologically classified as early spirals. This is probably because of the extended halo usually found in these objects which could be interpreted as a disc component by the automated algorithms.

Despite the fact that we see some differences between the different selections, the fit parameters are roughly consistent within 1σ. Since a Sérsic index based selection contains an important fraction of star-forming galaxies ($\sim$50 per cent; a population which presents, on average, higher sizes than ETGs; e.g. Mei et al. 2012), this population tends to increase the scatter of the relation.

A similar behaviour is observed if we select galaxies just based on the morphology (ETGs, Fig. 8). The scatter of the relation might be increased by the presence of a star-forming population of galaxies with early-type morphology. Even if the number densities of these objects are small in the local universe (e.g. Kannappan, Guie & Baker 2009) they tend to increase at high z (e.g. Huertas-Company et al. 2010) and might have a consequence on the size measurements.

We quantify the possible effects of galaxy selection in Fig. 9 where we plot the mass-normalized radius ($r_e \times (10^{11}\,M_\odot/M_*)$) evolution for different galaxy selections (ETG, passive ETGs, $n > 2.5$, passive galaxies) with $\log(M/M_\odot) > 10.7$ (the mass selection
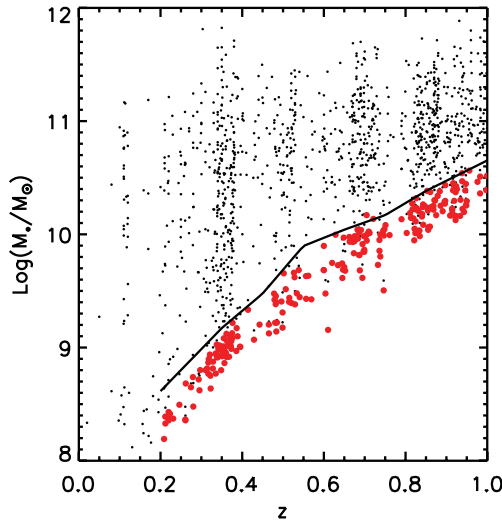
Figure 4. Stellar mass as a function of redshift of passive ETGs. The red filled big circles are M_*^{lim} and the black line shows the 95 per cent completeness level. See the text and Pozzetti et al. (2010) for more details.
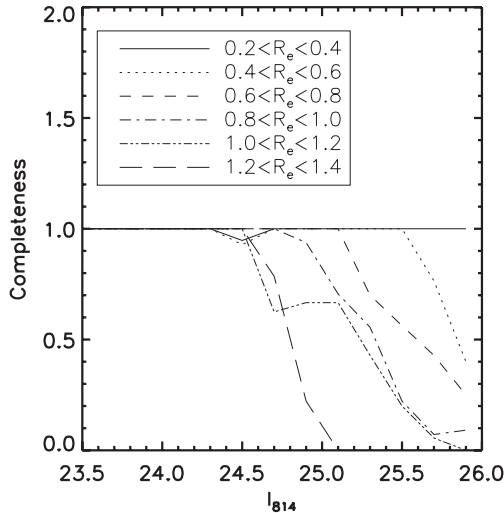
Figure 5. Completeness of our sample as a function of magnitude and size in arcseconds (see the text for details). Objects with $F814W < 24$ are all detected.

for this figure is chosen to match the one from Newman et al. 2012). We observe that surprisingly, the differences between the different selection in terms of size evolution are negligible and also consistent with recent results (i.e. Damjanov et al. 2011; Cimatti et al. 2012; Newman et al. 2012). We can conclude that these different selections usually found in the literature lead to similar results.

In this work, we have an additional ingredient though, usually lacking in previous published results which is the morphological dissection of passive galaxies as explained in Section 2.3. As a matter of fact, the population of passive galaxies is not a homogeneous population of objects. We show indeed some example stamps of massive ($\log(M/M_\odot) > 10.5$) passive galaxies with different morphologies in Fig. 10. It is easy to note by simple visual inspection that not all passive galaxies are bulge dominated. The relative abundance of each morphological type as a function of stellar mass is quantified in Fig. 11, for all our passive galaxy sample.

As expected, early-type morphologies dominate the population of passive galaxies up to $z \sim 1$ at all stellar masses, being about

80 per cent of the total population at all redshifts. The remaining 20 per cent is populated by early-type spirals while late-type spiral fractions are negligible. At all redshifts up to $z \sim 1$, elliptical galaxies dominate the ETG population at masses $\log(M/M_\odot) > 11-11.2$. At $z < 0.5$, galaxies with masses $\log(M/M_\odot) < 11$ are around half ellipticals and half lenticular, while lenticulars dominate the low-mass fractions at $z > 0.5$. In other words, an important fraction of passive galaxies from $z \sim 1$ (if not the majority) could have a disc component (see also Bundy et al. 2010; van der Wel et al. 2011; Mei et al. 2012). We also show in Appendix A, a version of Fig. 11 obtained with the two independent visual classifications performed in this work. One of the classifiers (SM) finds visually more Sas than S0s with respect to the automated classification, specially at high redshift. However, the separation between galaxies with disc (Sas and S0s) and without disc (ellipticals) is very similar to what is obtained with the automated classification, except that elliptical galaxies are not dominant at the high-mass end in the highest redshift bin, which is also found by the second classifier (MHC).

Studying the size evolution of *passive galaxies all together* (as often done in several works), mixes not only ETGs with early spirals (*Sab*), but also ETG with different morphological populations (e.g. ellipticals and lenticulars) for which the evolution is not necessarily of the same nature.

Differences in the mass–size relation of ellipticals and lenticulars are visible in Figs 6–8 and Table 1. S0 galaxies tend to be not only less massive but also more compact with respect to ellipticals.

In the next sections, we will focus on the sample of passive galaxies [sample (i)] and will quantify these differences by studying the dependence of the size evolution of passive galaxies on different morphological types (namely ellipticals and lenticulars). The final sample contains 404 group (232 within $0.5 \times R_{200C}$ and with $P_{\mathrm{MEM}} > 0.5$) and 459 field galaxies.

### 3.2 Size growth of passive galaxies with different morphologies from $z \sim 1$

Throughout this section, we normalize sizes using the local reference derived by Bernardi et al. (2010) on the SDSS using a clean sample of elliptical galaxies (excluding S0s). We paid special attention in properly calibrating the local reference to be as consistent as possible with our high-redshift measurements. We checked for that purpose that our low-redshift ($z < 0.3$) data are consistent at 1σ with their local mass–size relation which confirms that both relations are well calibrated. Sizes in each redshift bin are computed by fitting a 1D Gaussian function to the size ratio distributions and keeping the position of the peak as the adopted value. Results remain however unchanged if we use instead a classical median or a 3σ clipped average. Uncertainties are computed through bootstrapping, i.e. we repeat the computation of each value 1000 times removing one element each time and compute the error as the 1σ error of all the measurements.

In this section, since we are mainly interested in the effects of different morphologies, we mix group (larger selection) and field galaxies in a single population to improve statistics. Both populations will be considered separately in Section 3.3 in which we study the effects of environment in the mass–size relation.
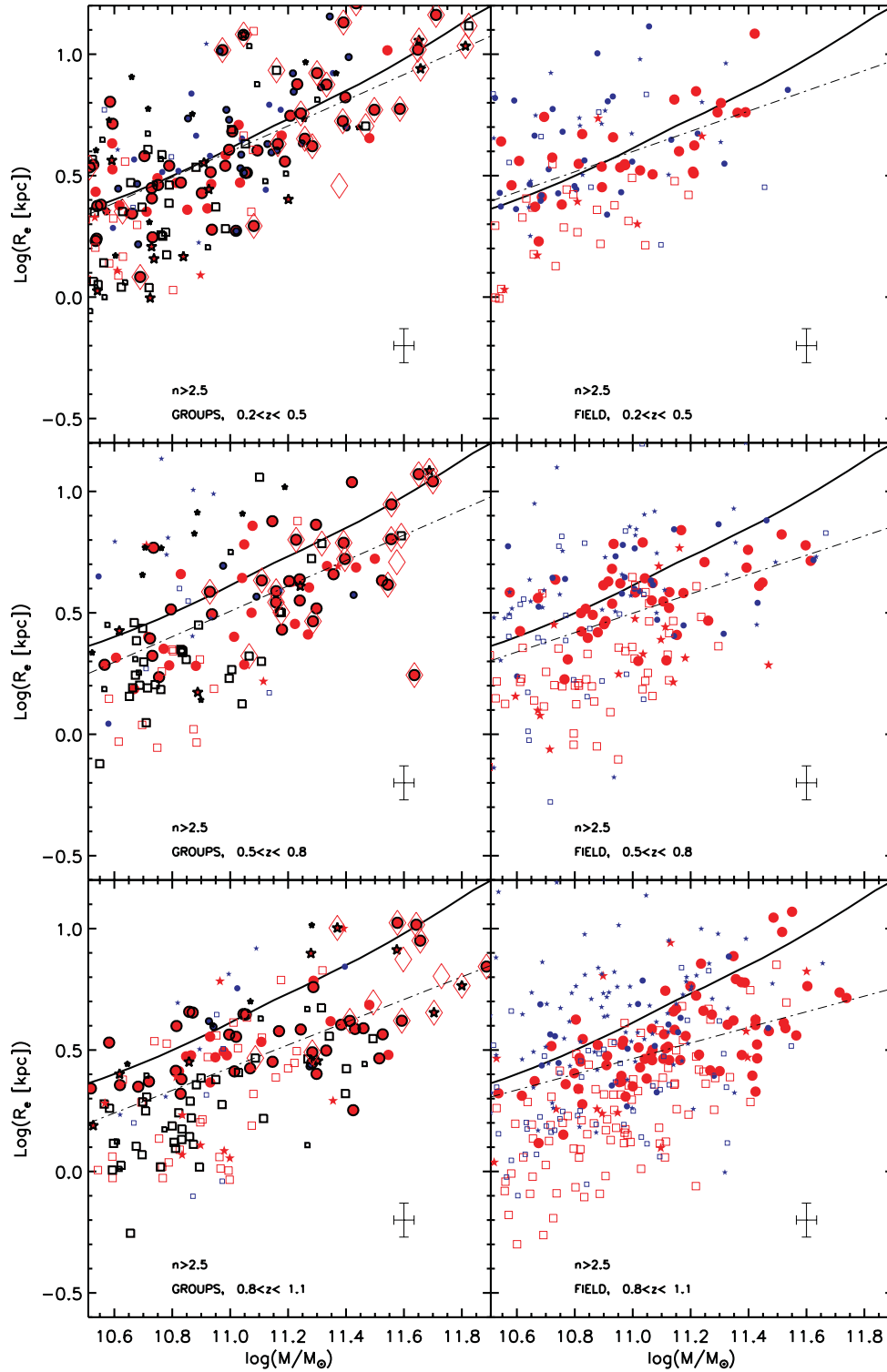
3.2.1 Ellipticals

In Fig. 12, we show the size evolution of ellipticals as compared to lenticulars in two mass bins ($10.5 < \log(M/M_\odot) < 11$ and $11.0 <$
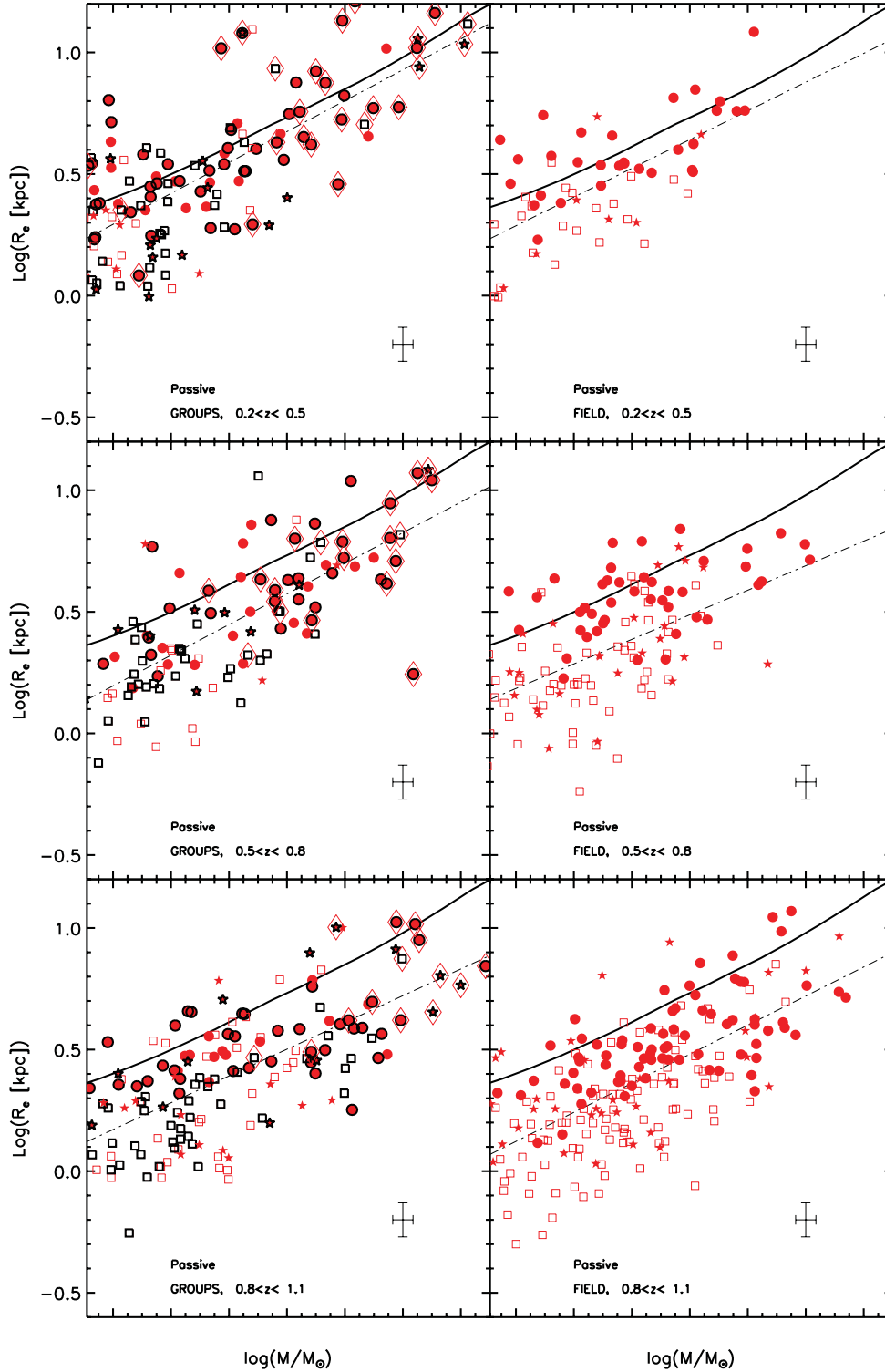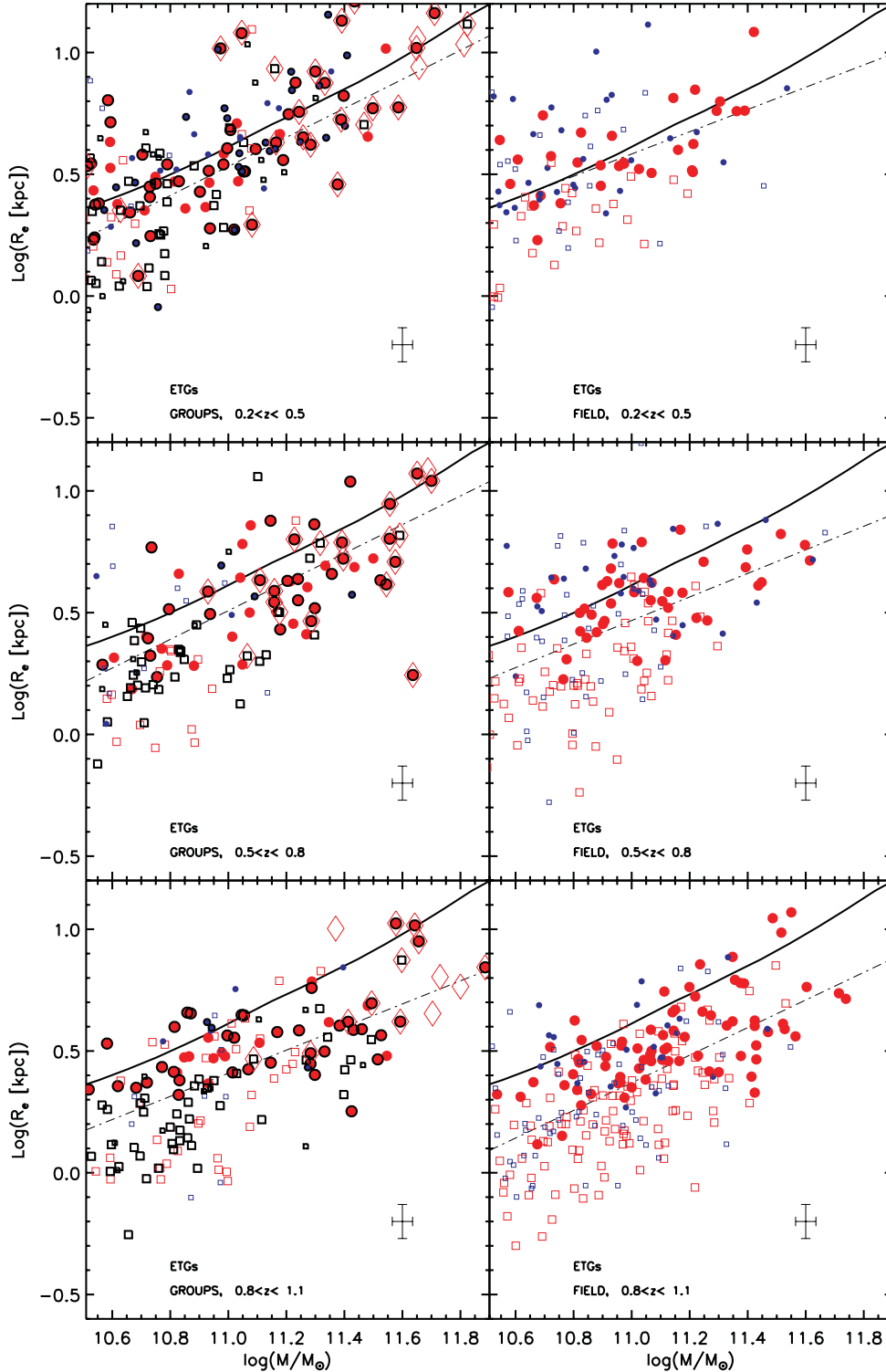
Figure 6. Mass–size relation of passive galaxies in groups (left-hand column) and field environments (right-hand column). The filled circles are ellipticals, the empty squares are lenticulars and the stars are late-type galaxies (including early- and late-type spirals). The symbols with a black contour show *central* group members ($r < 0.5 R_{200C}$ and $P_{MEM} > 0.5$). The diamonds show the position of BGGs. We also show on the bottom-right corner the typical error bars for sizes and stellar masses. The solid line shows the local relation as measured by Bernardi et al. (2010) and dash–dotted lines are the best fits to the whole passive population. The distribution in the mass–size plane of the different morphological types are not the same. A pure *star formation* selection does not ensure that we are studying just bulge growth but also galaxies with a disc component which might follow a different evolutionary path.

Figure 7. Mass–size relation of $n > 2.5$ galaxies in groups (left-hand column) and field environments (right-hand column). The filled circles are ellipticals, the empty squares are lenticulars and the stars are late-type galaxies (including early- and late-type spirals). The symbols with a black thick contour show *central* group members ($r < 0.5 R_{200C}$ and $P_{MEM} > 0.5$). The diamonds show the position of BGGs. Blue small/red big symbols show active/passive galaxies, respectively. We also show on the bottom-right corner the typical error bars for sizes and stellar masses. The solid line shows the local relation as measured by Bernardi et al. (2010) and dash–dotted lines are the best fits to the whole $n > 2.5$ population. A Sérsic index based selection contains an important fraction of star-forming galaxies which tend to increase the scatter of the relation. The effect seems to be more pronounced in the field population so it could yield to observed differences in the evolution of the mass–size relation with environment.

Figure 8. Mass–size relation of ETGs in groups (left-hand column) and field environments (right-hand column). The filled circles are ellipticals and the empty squares are lenticulars. The symbols with a black thick contour show *central* group members ($r < 0.5\,R_{200C}$ and $P_{MEM} > 0.5$). The diamonds show the position of BGGs. The blue small/red big symbols show active/passive galaxies, respectively. We also show on the bottom-right corner the typical error bars for sizes and stellar masses. The solid line shows the local relation as measured by Bernardi et al. (2010) and dash–dotted lines are the best fits to the whole early-type population.

$\log(M/M_{\odot}) < 11.5$. The upper limit is chosen because there are almost no S0s with masses greater than $10^{11.5}$ M$_{\odot}$ (see Fig. 2) and we want to compare the evolution of the two morphological types in the same mass ranges.

Ellipticals in the mass range $11.0 < \log(M/M_{\odot}) < 11.5$ experienced a ~40 ± 10 per cent size growth from $z \sim 1$ to present. We find an α value of $\alpha = 0.8 \pm 0.28$ when fitting the evolution with a power law ($r_e \propto (1 + z)^{-\alpha}$). However, the most relevant feature is that, as

Table 1. Power-law fitting parameters to the mass–size relation ($r_e = (\frac{M}{M_\odot})^a + b$) for different galaxy selections and environments. Pall stands for *Passive all* [sample (i) from the text], PEs is *Passive ellipticals*, PS0s means *Passive lenticulars*, $n > 2.5$ are galaxies from a Sérsic based selection [sample (ii)] and ETGs stands for early-type galaxies independently of star formation [sample (iii)]. N is the number of objects in each bin with $\log(M_*/M_\odot) > 10.5$.

Redshift	Environment	Sample	a	log(b)	N
$0.2 < z < 0.5$	Group	Pall	0.52 ± 0.03	-5.25 ± 0.34	128
		PEs	0.47 ± 0.04	-4.65 ± 0.49	65
		PS0s	0.49 ± 0.05	-4.91 ± 0.57	43
		$n > 2.5$	0.52 ± 0.05	-5.21 ± 0.37	263
		ETGs	0.59 ± 0.06	-6.02 ± 0.66	133
	Field	Pall	0.59 ± 0.09	-5.9 ± 0.99	59
		PEs	0.41 ± 0.04	-4.65 ± 0.49	30
		PS0s	0.49 ± 0.05	-4.91 ± 0.57	22
		$n > 2.5$	0.41 ± 0.05	-3.98 ± 0.56	161
		ETGs	0.45 ± 0.08	-4.44 ± 0.92	99
$0.5 < z < 0.8$	Group	Pall	0.56 ± 0.04	5.27 ± 0.45	110
		PEs	0.40 ± 0.07	-3.85 ± 0.8	52
		PS0s	0.51 ± 0.06	-5.27 ± 0.72	46
		$n > 2.5$	0.58 ± 0.05	-5.24 ± 0.52	176
		ETGs	0.58 ± 0.06	-5.97 ± 0.66	155
	Field	Pall	0.50 ± 0.11	-5.16 ± 1.27	123
		PEs	0.27 ± 0.07	-3.85 ± 0.8	43
		PS0s	0.51 ± 0.06	-5.27 ± 0.72	54
		$n > 2.5$	0.39 ± 0.04	-3.88 ± 0.49	250
		ETGs	0.48 ± 0.07	-4.85 ± 0.78	158
$0.8 < z < 1.0$	Group	Pall	0.49 ± 0.04	-4.98 ± 0.41	155
		PEs	0.35 ± 0.05	-3.38 ± 0.60	53
		PS0s	0.42 ± 0.05	-4.37 ± 0.57	73
		$n > 2.5$	0.46 ± 0.04	-4.71 ± 0.46	209
		ETGs	0.47 ± 0.05	-4.81 ± 0.59	148
	Field	Pall	0.59 ± 0.05	-6.21 ± 0.52	210
		PEs	0.43 ± 0.05	-3.38 ± 0.60	65
		PS0s	0.42 ± 0.05	-4.37 ± 0.57	99
		$n > 2.5$	0.32 ± 0.03	-3.07 ± 0.41	394
		ETGs	0.56 ± 0.04	-5.86 ± 0.51	252

shown in the left-hand panel of Fig. 12, below $\sim 10^{11}$ M$_\odot$, elliptical galaxies do not experience a significant size growth, e.g. their size does not evolve in a significant way with respect to local ellipticals from the SDSS ($r_e \propto (1 + z)^{-0.34 \pm 0.17}$; see also Raichoor et al. 2012 for similar results at higher redshift). The mass dependence is even more clear in Fig. 13 in which we show in the left-hand column, the observed size evolution for ellipticals in three bins of increasing stellar mass [$10.5 < \log(M/M_\odot) < 11, 11 < \log(M/M_\odot) < 11.2$ and $11.2 < \log(M/M_\odot) < 12$]. The derived α value parametrizing the evolution is $\alpha = 0.34 \pm 0.17$, 0.63 ± 0.18 and 0.98 ± 0.18 from low to high mass, showing a clear increasing trend with stellar mass. In Appendix A, we show that when using visual morphological classifications the evolution in the low-mass bin is stronger (~ 30 per cent) making the difference between the two first mass bins less pronounced. The trend is still preserved though (see Table A1), specially between the last two bins. One possible source of error though is that the stellar mass bins used are comparable to the expected error of the stellar mass (i.e. 0.2 dex), so the different behaviours found can be affected by contaminations of objects with lower/higher stellar masses. We have run Monte Carlo simulations to check if the trends found are preserved with typical errors expected on the stellar mass. For that purpose, we added to every stellar mass a random shift within 3σ of the expected error in stellar mass and recomputed the median sizes 1000 times. The values

found are consistent at 1σ level so we do not expect a significant contribution of this effect in our measurements.

Interestingly, this mass dependence is less pronounced when studying all ETGs or passive galaxies as a whole (right-hand column of Fig. 13). The best-fitting relations for this whole sample are $r_e \propto (1 + z)^{-1.01 \pm 0.23}$ for ETGs with stellar masses $10.5 < \log(M/M_\odot) < 11$ and $r_e \propto (1 + z)^{-1.21 \pm 0.22}$ and $r_e \propto (1 + z)^{-1.19 \pm 0.18}$ for $11 < \log(M/M_\odot) < 11.2$ and $11.2 < \log(M/M_\odot) < 12$, respectively, which are fully consistent within 1σ.

The mass dependence has been discussed in the recent literature providing different results. Williams et al. (2010) and Ryan et al. (2012) measured a mass dependence similar to the one reported here for ellipticals, i.e. with the evolution being stronger at higher stellar masses, while other works like Damjanov et al. (2011) suggest that the slope of the mass–size relation is mass independent. We show here that the results might depend on how the selection is performed. When selecting pure passive bulges a mass dependent evolution seems to emerge. As a matter of fact, Williams et al. (2010) select passive galaxies based on the specific star formation rate (instead of the red sequence for other works). They might be removing from their sample more *discy* galaxies (also removed from our elliptical sample and not from an ETG sample) which could explain that we find similar results. Note also that for galaxies
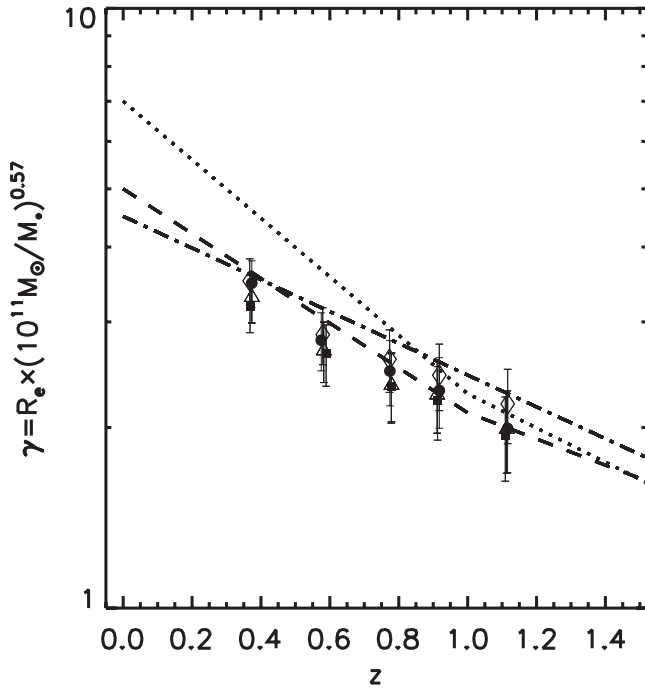
Figure 9. Mass-normalized radius for our sample for galaxies with masses $\log(M/M_\odot) > 10.7$, as a function of redshift for different selections compared to recent published results. The circles are ETGs, the squares passive galaxies, the triangles passive ETGs and the diamonds $n > 2.5$ galaxies. The dashed line shows the Cimatti et al. (2012) fit, the dot–dashed line shows the Newman et al. (2012) fit and the dotted line shows the Damjanov et al. (2011) fit. Samples selected using the Sérsic index tend to show larger sizes, because of the contamination from passive spirals, which is larger in field samples. However, these differences are within 1σ.

with $\log(M_*/M_\odot) > 11.2$, the contribution from discy galaxies is almost zero and therefore selecting ETGs or ellipticals has almost no effect in the size evolution. The strong size evolution found for these galaxies is therefore robust to galaxy selections and will be discussed in detail in Section 4.

3.2.2 Lenticulars and early spirals

The bottom panels of Fig. 12 show the size evolution of lenticular galaxies in two mass bins normalized to the same local relation. They appear on average more compact than ellipticals, in a similar way as in the local Universe, as shown in Section 2.3 and confirming the fact already pointed out by van der Wel et al. (2011) that the most compact galaxies at high redshift have a disc component (this effect is preserved even when not circularizing the radii). Since we normalize with the same local relation as for ellipticals, we also plot, for reference, the ratio of lenticular sizes over those of the ellipticals in the SDSS (note that all fractions are normalized to the local SDSS elliptical sizes).

What is interesting is that the size growth of lenticulars does not seem to depend significantly on stellar mass given the large uncertainties, contrary to the behaviour shown for the elliptical population: $r_e \propto (1 + z)^{-0.67\pm0.30}$ and $r_e \propto (1 + z)^{-1.02\pm0.25}$ for low mass and massive lenticulars, respectively.

In order to further investigate what is driving the size increase in these galaxies, we made a simple exercise which is to compare the observed evolution to the one expected in a star-forming disc-dominated population. We selected for that purpose, galaxies in our sample with $M(NUV) - M(R) < 3.5$ and a spiral-like morphology
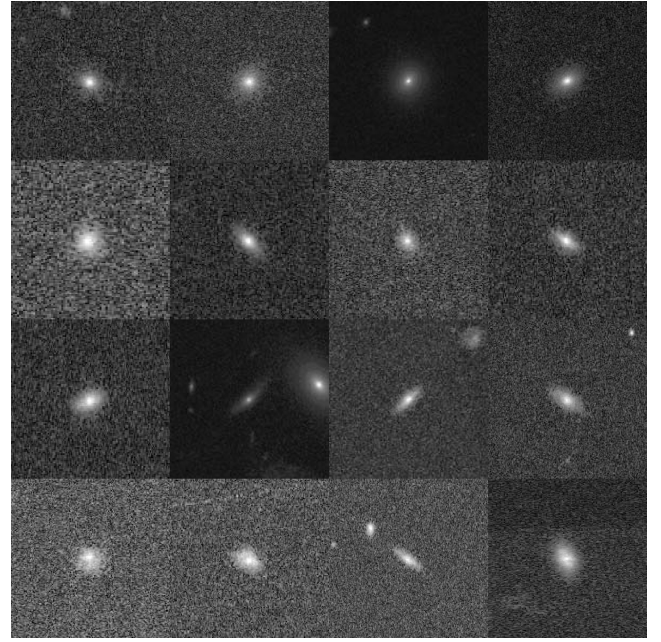
Figure 10. Example stamps of passive galaxies of four morphological classes. First row: ellipticals, second row: S0s, third row: early spirals and last row: late spirals. Stamp sizes are: 1 arcsec × 1 arcsec.

$[max(P(E), P(S0), P(Sab), P(Scd)) = P(Sab)$ or $max(P(E), P(S0), P(Sab), P(Scd)) = P(Scd)]$, and computed the size growth as a function of redshift as we did for the S0s. Since the overall sizes of late-type galaxies are larger than ETGs (see also Mei et al. 2012), we divide the overall relation by a factor of 1.3 so that the values at $z = 0$ agree (see Fig. 12). We just plot the relation for the low-mass end because there are not enough high-mass late type to derive a reliable relation at high masses.

Even though the normalization for discs is still slightly higher, the trends of the size growth for the two populations are very similar ($r_e \propto (1 + z)^{-0.67\pm0.30}$ for lenticulars and $r_e \propto (1 + z)^{-0.54\pm0.44}$ for star-forming discs) which suggests that the size growth of a large part of the ETGs and that of the late-type galaxies evolve at similar rates. If we add to the passive S0 population, also passive early-type spirals ($max(P(E), P(S0), P(Sab), P(Scd)) = P(Sab)$ and $M(NUV) - M(R) > 3.5$) the trend is preserved.

3.3 Environment

We now study the effect of environment on the mass–size relation of galaxies paying special attention to the uncertainties due to the galaxy sample selection.

Fig. 14 shows the evolution of mass-normalized radii γ for $\log(M_*/M_\odot > 10.7)$ passive ETGs in groups and in the field. In the right-hand panel we show only group members with a probability greater than 0.5 and within $0.5 \times R_{200C}$ from the group centre (central selection) to make sure that the signal is not washed out by interlopers. No significant differences are observed between the central and the larger sample. Our main result is therefore that the mass–size relation does not depend on environment for field and groups with halo masses $M_{200C}/M_\odot < 10^{14.22}$. Fig. 15 also shows the evolution of the size of field and group passive galaxies divided into the same morphological and stellar mass bins as in the previous section. Relations are more scattered because of the Poisson noise
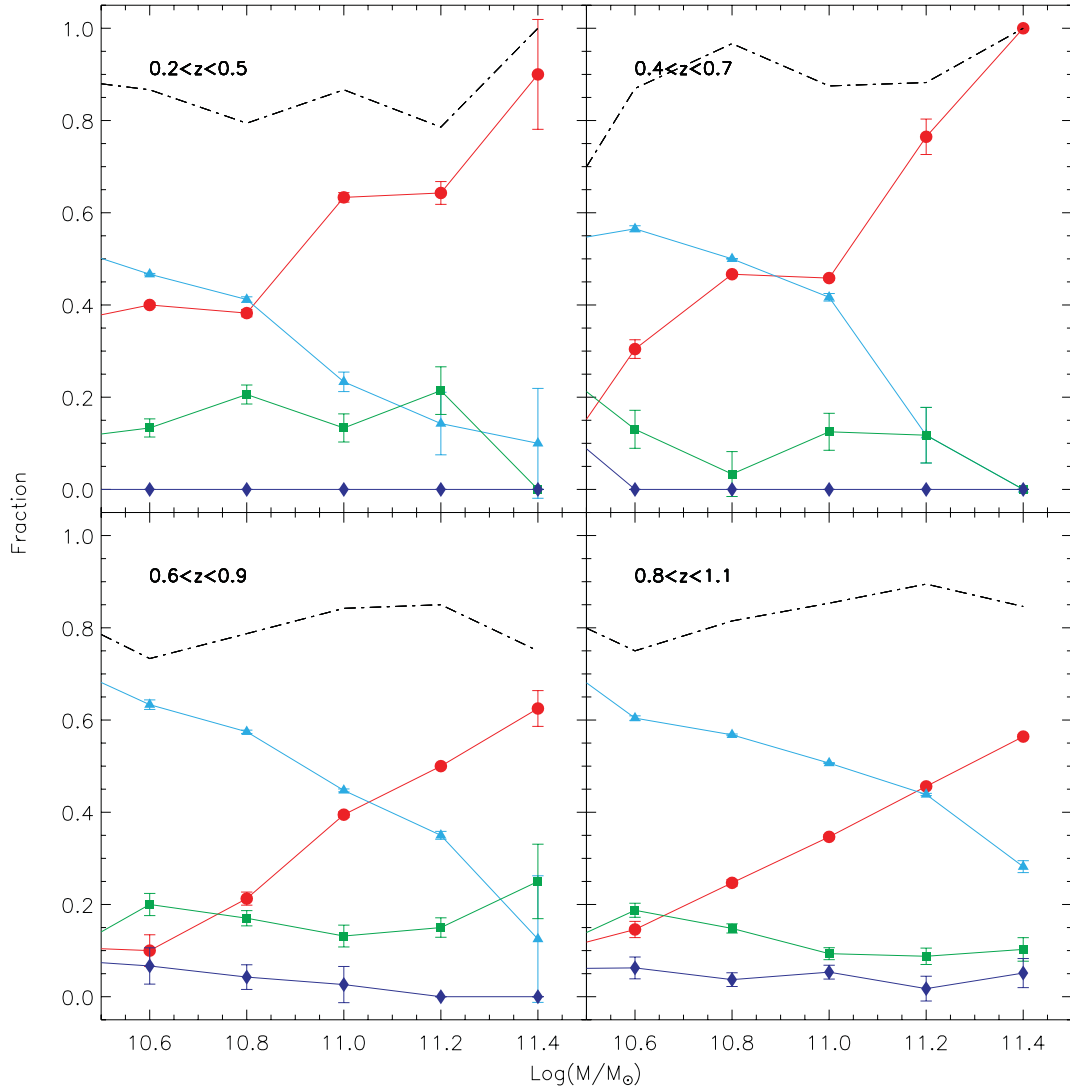
Figure 11. Morphological fractions of passive galaxies as a function of stellar mass and redshift. Red circles: ellipticals, cyan triangles: S0s, green squares: early spirals, blue diamonds: late spirals. The black dashed line shows the fraction of ETGs (ellipticals and S0s together). The uncertainties are calculated following Gehrels (1986; see Section 3 for binomial statistics; see also Mei et al. 2009). These approximations apply even when ratios of different events are calculated from small numbers, and yield the lower and upper limits of a binomial distribution within the 84 per cent confidence limit, corresponding to 1σ. Note that using this conservative approach our uncertainties are slightly overestimated (Cameron et al. 2011).

(especially for massive lenticulars) but we do recognize the same trends as for the mixed population.

A point to take into account when normalizing with the local relation is the fact that groups and field galaxies in the local universe could follow different mass–size relations. We have checked this point by comparing the median mass–size relation of ETGs in groups from the Yang et al. (2007) catalogue to the full DR7 sample. Yang et al. (2007) put together a catalogue of ∼300 000 groups detected in the SDSS DR4 using an automated halo-based group finder. For this work, we restricted to groups with more than two members and removed those objects affected by edge effects ($f_{\rm edge} < 0.6$). According to their fig. 2, ∼80 per cent of the groups have ∼20 per cent contamination which is comparable to the expected contamination in our sample. We use as halo mass estimate, HM1, which is based on the characteristic luminosity of the group but results remain unchanged when using a halo mass estimate based on the characteristic stellar mass. The group catalogue has been correlated with the catalogue of 2D Sérsic decompositions

by Simard et al. (2011) to get a size estimate for all our galaxies (circularized effective radius of the best fit) as well as with the morphological catalogue by Huertas-Company et al. (2011) to select ETGs ($P_{\rm early} > 0.8$). The mass–size relations that we obtained for the field and group galaxies are fully consistent within 1σ; we therefore use the same local relation to normalize group and field sizes.

In Raichoor et al. (2012), in a sample dominated by galaxies with $10 < \log(M/M_\odot) < 11$, we have noted that while differences in median/average sizes cannot distinguish early-type populations in different environments, a test on both the mean and scatter of their distribution can point out environmental differences.

We extend Kuiper and Kolmogorov–Smirnoff (KS) tests analysis to our group and field passive ETG size distribution in different mass bins to test environmental dependences on their distribution scatter that might distinguish size evolution in the groups and the field. We divide our sample in three redshift bins ($0.2 < z < 0.5$, $0.5 < z < 0.8$ and $z > 0.8$) and two mass bins ($10.5 < \log(M/M_\odot) < 11$
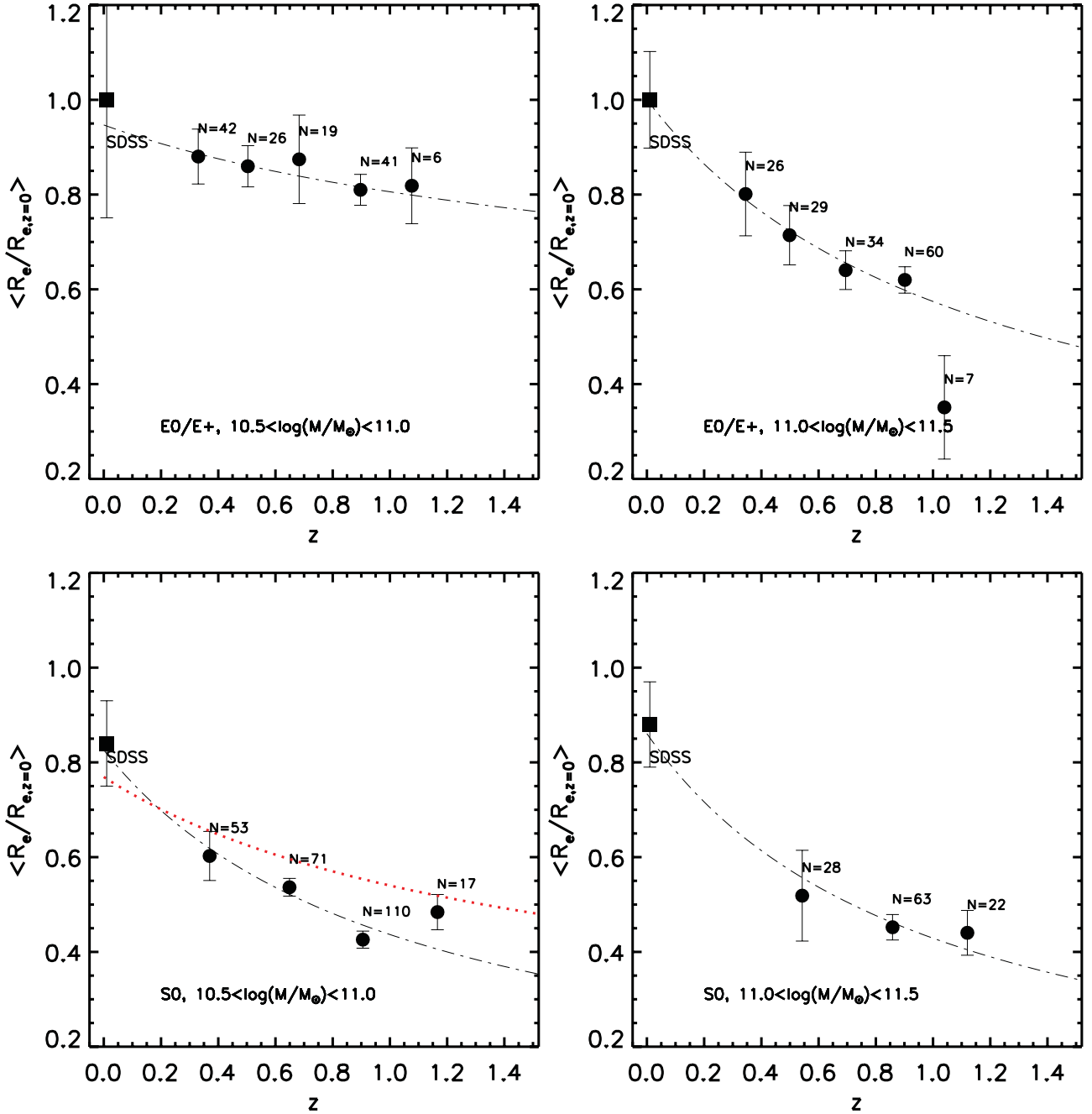
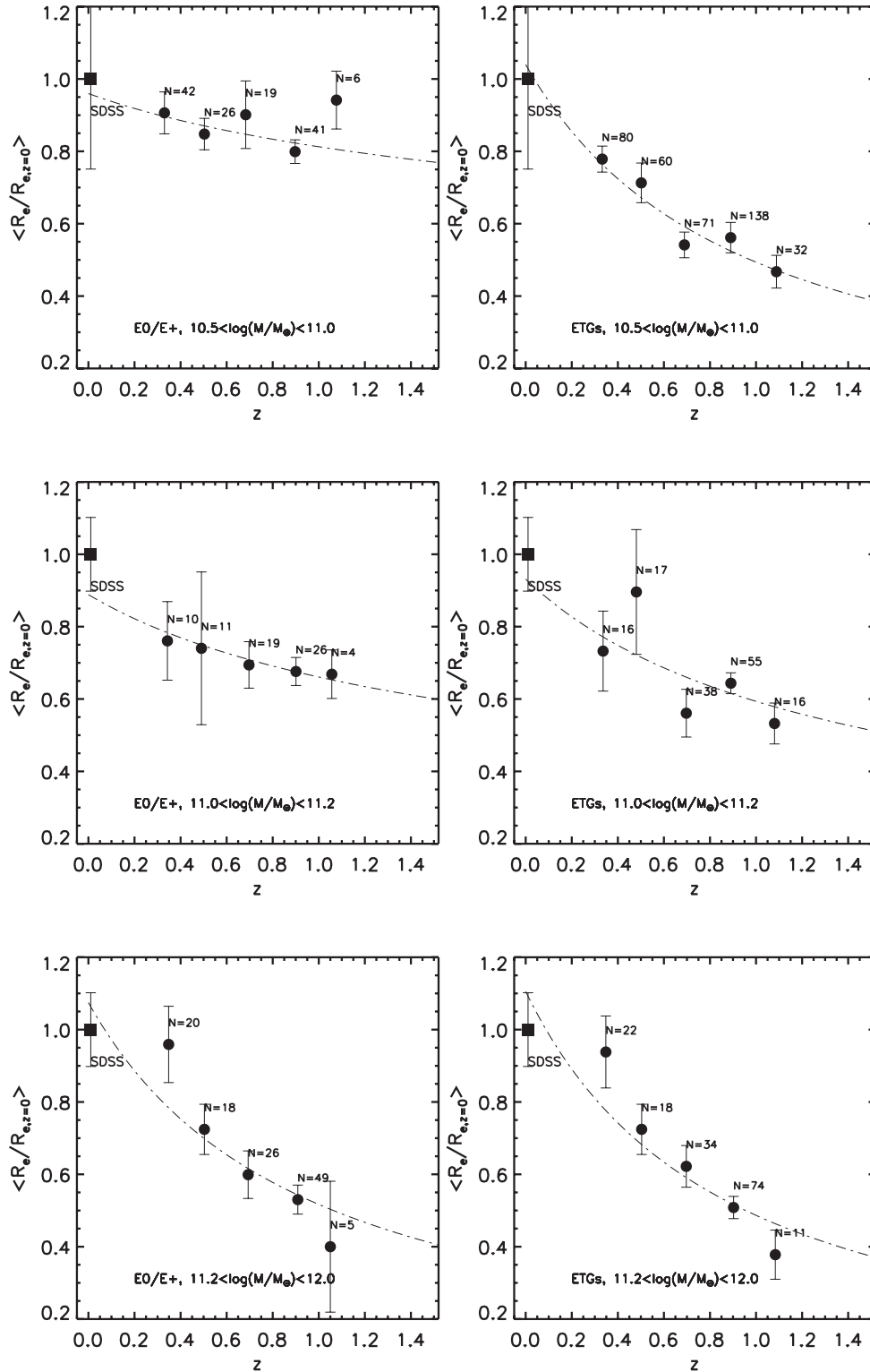**Figure 12.** Size evolution of passive elliptical (top) and S0 (bottom) galaxies in two mass bins. Left-hand panel: $10.5 < \log(M/M_\odot) < 11$, right-hand panel: $\log(M/M_\odot) > 11.2$. The dot–dashed lines are the best-fitting lines and the red dotted line in the bottom-left panel is the measured evolution of star-forming galaxies (see the text for details). Numbers indicate the number of objects in each redshift bin. Error bars are the scatter of the distributions. SDSS points are computed using the catalogues from Nair & Abraham (2010) and Simard et al. (2011).

and $\log(M/M_\odot) > 11$) and performed the tests for the two group selections.

Results of the analysis are summarized in Table 2 and the different size distributions for several sample selections are shown in Fig. 16. Same results for the central selection are shown in the appendix. For all redshift and mass bins, both the KS and Kuiper test results almost always give a probability >80 per cent that field and groups size ratios are drawn from the same distribution even when considering only group members with $P_{MEM} > 0.5$ and close to the group centre.

Recent works at similar redshifts have found that galaxy size evolution depends on environment. Cooper et al. (2011) find indeed

that denser environments at $z < 1$ tend to be populated by larger galaxies. Differences with this work can come from the way environment is measured and/or how galaxy selection is performed. Cooper and collaborators selection is indeed based exclusively on the Sérsic index, which as shown in Fig. 7 leads to the inclusion of some star-forming galaxies which tend to increase the scatter of the field population. As a matter of fact, we find that KS and Kuiper tests applied to the size distributions of group and field galaxies selected on the basis of the Sérsic index do show that the distributions have probabilities <50 per cent to be drawn from the same distributions. However, median sizes do not change

Figure 13. Size evolution of elliptical (left-hand column) and early-type passive galaxies (right-hand column) in three mass bins. Top row: $10.5 < \log(M/M_\odot) < 11$, middle row: $11.0 < \log(M/M_\odot) > 11.2$ and bottom row: $11.2 < \log(M/M_\odot) > 12$. Numbers indicate the number of objects in each redshift bin. Error bars are the scatter of the distributions.

significantly so this fact cannot fully explain the difference between the two works. Concerning the environment measurement, we use here the DM halo mass as primary environment estimator whereas Cooper and collaborators use the local density based on neighbours.

3.3.1 BGGs

BGGs deserve a particular mention since they have been more studied because of their very particular position at the centre of massive structures and their high surface brightness which make
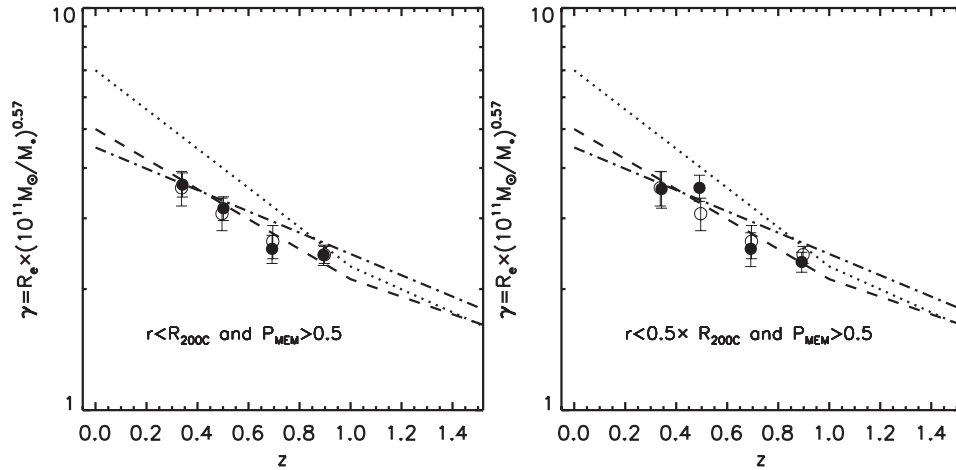
Figure 14. Mass-normalized radius for quiescent ETGs in different environments for galaxies with masses $\log(M/M_\odot) > 10.7$, as a function of redshift. The filled circles are ETGs living in groups and the empty circles are in the field. The left-hand panel shows all group members within $r < R_{200C}$ and a probability to be in the group larger than 0.5 and the right-hand panel shows the result with a more conservative group selection, i.e. $r < 0.5 \times R_{200C}$ and $P_{MEM} > 0.5$. The dashed line shows the Cimatti et al. (2012) fit, the dot–dashed line shows the Newman et al. (2012) fit and the dotted line shows the Damjanov et al. (2011) fit. Samples selected using the Sérsic index tend to show larger sizes, because of the contamination from passive spirals, which is larger in field samples. However, these differences are within 1σ.

them easy to detect and analyse. Current works, though, do not agree about the BCG size evolution and how BCG sizes compare to those of field and satellite galaxies.

Based on SDSS data, Bernardi (2009) found that BCGs are larger than field and satellite galaxies at fixed stellar mass and that there is a steep evolution of their size from $z \sim 0.3$ to present. The author also argues that minor dry mergers are the most probable mechanism to explain the build-up of these objects. Also in the SDSS, Weinmann et al. (2009) did not find a significant difference between the sizes of centrals and satellites in groups.

At higher z, Ascaso et al. (2011) find a significant size evolution from $z \sim 0.6$ to present, but do not detect any evolution in their profile. They interpret this fact as a signature of feedback instead of merging. Stott et al. (2011) studied a sample of high-redshift BCGs and found a very mild evolution of the BCG size from $z \sim 1$.

From the modelling point of view, Shankar et al. (2011) showed that BCGs should evolve much faster than satellite galaxies.

We use the BGGs definition as the most massive galaxies within an NFW scale radius of the X-ray position, from the George et al. (2011) catalogue. Fig. 17 shows the size evolution for passive BGGs and satellite group members with similar stellar mass ($\log(M/M_\odot > 11$). We find that the two population evolve in a similar way within the error bars, e.g. we do not observe significant differences in the size evolution of BCGs as compared to satellite group members with similar stellar mass.

4 DISCUSSION

To understand why not all populations evolve in the same way, we consider different scenarios of galaxy growth. There are two main, well distinct, physical mechanisms proposed so far in the literature to puff up massive bulges from high redshifts to the local Universe: galaxy mergers and mass-loss via quasar and/or stellar wind.

4.1 Mergers

Hierarchical models of structure formation envisage the growth in size of massive galaxies via a sequence of major and minor mergers. While (mainly gas-rich) major mergers are believed to happen at

high redshifts and may be responsible for forming the galaxy, minor dry merger happen on cosmological time-scales and tend to impact mainly the external regions of the galaxy, thus increasing its size, but leaving its inner regions mostly unaltered.

In this work, we consider the predictions of several, representative, hierarchical galaxy evolution models that differ in terms of underlying techniques and physical assumptions. We adopt, more precisely, the models by Bower et al. (2006), Hopkins et al. (2009), Guo et al. (2010) and Shankar et al. (2011). All model predictions have been computed for the range of stellar masses[2] and galaxy type of interest to this paper. We mainly considered galaxies with $B/T > 0.5$ when comparing to ETGs (though we checked that our results are practically unchanged when restricting to $B/T > 0.7$), and galaxies with $0.3 < B/T < 0.7$ when comparing to S0s.

Both the Bower et al. (2006) and Guo et al. (2010) models follow the hierarchical growth of galaxies along the merger trees of the Millennium simulation (Springel et al. 2005). Galaxy progenitors are initially disc-like and after a major merger the remnant is considered to be an elliptical (though disc regrowth can happen). Minor mergers instead tend to preserve the initial morphology of the most massive progenitor but tend to increase the mass of the bulge and disc components via the aggregation of old stars and newly formed ones during the merger. Half-mass–sizes are then updated at each merger event assuming energy conservation. Despite being built on the same DM simulation, the subhalo/galaxy merger rates of these two models differ due to the different corrections in dynamical friction time-scales. In both models, bulges can also grow via disc instabilities. However, the implementation of the latter physical ingredient substantially differs in the two models, with Bower et al. (2006) assuming a much stronger bulge growth via disc instabilities with respect to the Guo et al. (2010) model (see discussion in Shankar et al. 2011). Most importantly for size evolution, both models do not consider gas dissipation during gas-rich major mergers, a feature that has instead been included by Shankar et al. (2011) by properly adapting the Guo et al. (2010) model. The Hopkins

---

[2] All predictions have been corrected to a common Chabrier IMF. We however expect differences in the IMF to have a minor impact on the rate of size evolution of massive spheroids.
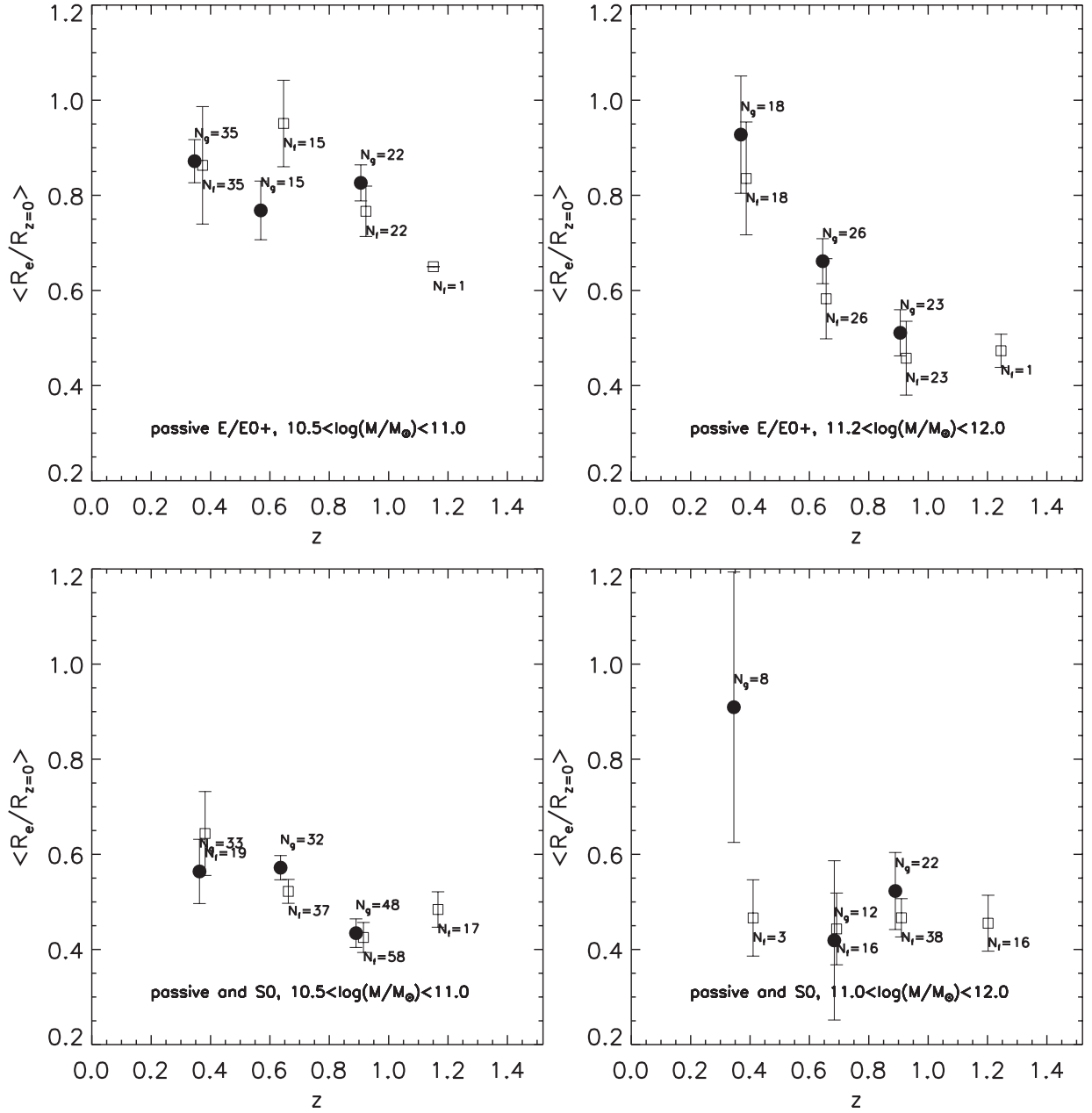
Figure 15. Evolution of the size of galaxies from our sample as a function of redshift referred to the local relation from SDSS (see the text for details). The filled circles are group galaxies and the empty squares are from the field. Error bars are related to the scatter of the size distribution (see the text) and numbers indicate the number of galaxies in each redshift bin in the group sample.

et al. (2009) model follows the analytic mass accretion histories of haloes and at each time step initializes central galaxies and infalling satellites according to empirical correlations inspired by halo occupation techniques and high-redshift data. Equivalently to the models discussed above, at each merger the half-mass radius is updated following energy conservation arguments, with also gas dissipation (see also Nipoti et al. 2012 for a more recent work adopting similar techniques). Hopkins et al. (2009) have mainly focused on ETGs (not lenticulars) with stellar masses above $M_* > 10^{10}\,\mathrm{M_\odot}$.

4.1.1 The size growth of ellipticals compared to model predictions

In Fig. 18, we compare our results with predictions from Shankar et al. (2011), Bower et al. (2006) and Guo et al. (2010). For el-

lipticals, we focus here on the lowest and highest stellar mass bins of Fig. 13, where the differences are stronger (i.e. $10.5 < \log(M/\mathrm{M_\odot}) < 11$ and $\log(M/\mathrm{M_\odot}) > 11.2$). The first relevant feature arising from the comparison is that most of the theoretical predictions are in agreement with the (mild) size evolution of ETG galaxies with stellar masses $M_* < 10^{11}$ (left-hand panel of Fig. 18) (specially taking into account the uncertainties due to morphological classifications). Merger models are therefore successful to predict the size evolution of these lower mass ellipticals.

More interestingly, despite the significant variance in the input parameters and/or physics most merger models seem to be unable to reproduce completely the fast drop in sizes for quiescent ellipticals with stellar masses $\log(M_*/\mathrm{M_\odot}) > 11.2$, especially at $z > 0.5$ (right-hand panel of Fig. 18). This is in line, and

Table 2. Results of Kuiper and KS statistical tests applied to group and field galaxies size ratio distributions in different samples (see the text for details). Pall stands for all passive galaxies, PEs are passive ellipticals and PS0s passive lenticulars. N_{group} and N_{field} indicate the number of galaxies in the group and field samples, respectively. Numbers (1) and (2) indicate if the group sample is taken at $r < R_{200C}$ (1) or at $r < 0.5 \times R_{200C}$ (see the text for details). We did not compute the statistical tests when the number of objects was below 10.

Redshift	$\log(M/M_\odot)$	Sample	KS	Kuiper	N_{group}	N_{field}
$0.2 < z < 0.5$	10.5–11	Pall–1	0.95	0.99	68	36
		Pall–2	0.85	0.97	33	36
		PEs–1	0.98	0.98	35	17
		PEs–2	0.34	0.51	17	17
		PS0s–1	0.75	0.96	33	19
		PS0s–2	–	–	6	19
	11–12	Pall–1	0.99	0.97	38	16
		Pall–2	0.99	0.99	22	16
		PEs–1	0.99	0.99	30	13
		PEs–2	0.99	0.99	17	13
		PS0s–1	–	–	8	3
		PS0s–2	–	–	1	3
$0.5 < z < 0.8$	10.5–11	Pall–1	0.43	0.71	47	57
		Pall–2	0.12	0.85	19	57
		PEs–1	0.92	0.99	15	20
		PEs–2	0.40	0.78	7	20
		PS0s–1	0.99	0.98	32	37
		PS0s–2	–	–	6	37
	11–12	Pall–1	0.80	0.98	49	39
		Pall–2	0.87	0.99	26	39
		PEs–1	0.93	0.99	37	23
		PEs–2	0.92	0.95	20	23
		PS0s–1	0.12	0.15	12	16
		PS0s–2	–	–	1	16
$0.8 < z < 1.0$	10.5–11	Pall–1	0.99	0.99	70	82
		Pall–2	0.42	0.99	24	82
		PEs–1	0.88	0.99	22	24
		PEs–2	0.88	0.99	9	24
		PS0s–1	0.99	0.99	48	58
		PS0s–2	0.88	1.00	10	58
	11–12	Pall–1	0.95	0.70	53	89
		Pall–2	0.55	0.98	29	89
		PEs–1	0.95	0.99	31	51
		PEs–2	0.54	0.98	21	51
		PS0s–1	0.55	0.91	22	38
		PS0s–2	–	–	7	38

further complements, the recent claims of a possible inefficiency of the puffing-up via mergers pointed out by Shankar et al. (2011), Cimatti et al. (2012) and Nipoti et al. (2012). Note that in this stellar mass bin, the contribution of S0 galaxies is almost negligible (see Fig. 13), so a similar behaviour is found when selecting all ETGs with $\log(M_*/M_\odot) > 11.2$ and should be independent of the morphological selection.

Nipoti et al. (2012) have recently shown the results of a merger model initialized via halo occupation techniques that, by neglecting dissipative processes and assuming only mergers with spheroids, maximizes the evolution in surface density. They conclude that minor and major mergers may not be sufficient to explain the observed size growth of ETGs (see also López-Sanjuan et al. 2012). An other work where the size growth since $z \sim 1$ is explained almost completely by mergers (Newman et al. 2012) has to assume very short merger time-scales (1 Gyr) and steep growth efficiency, optimistic with respect to observations (note in addition that the size evolution they measure is less steep than the one reported here though, because of the selection used, as shown in Sections 3.1 and 3.2). Oser et al. (2012) have recently analysed 40 cosmolog-

ical resimulations of individual massive galaxies with final $M_* > 6.3 \times 10^{10}\,M_\odot$, out of which 25 appear quiescent ETGs. While they claim a strong size evolution in the *cumulative* distribution of galaxies with present stellar mass $M_* > 6.3 \times 10^{10}\,M_\odot$, a close inspection of their fig. 1 (left-hand panel) reveals that galaxies above $M_* > 2 \times 10^{11}\,M_\odot$ have indeed had a rather mild size evolution at fixed stellar mass of about $\sim 30-40$ per cent at $z < 1$. Nevertheless, this may not necessarily reflect a failure of hierarchical models, as part of the discrepancy could simply arise from the specific underlying assumptions made. For example, the early semi-analytic model by Khochfar & Silk (2006) predicts a stronger size evolution for the very massive galaxies with $M_* > 5 \times 10^{11} \times M_\odot$, in better agreement with observations.

Overall, most merger models have some difficulties in fully reproducing the size evolution of the most massive ETGs. Part of the apparent evolution in sizes may be driven by relatively younger larger galaxies formed at later epochs (progenitor bias) even if the relevance of this effect is still unclear. A recent empirical model by López-Sanjuan et al. (2012), based on merger observations in the COSMOS field, shows in fact that taking into consideration major
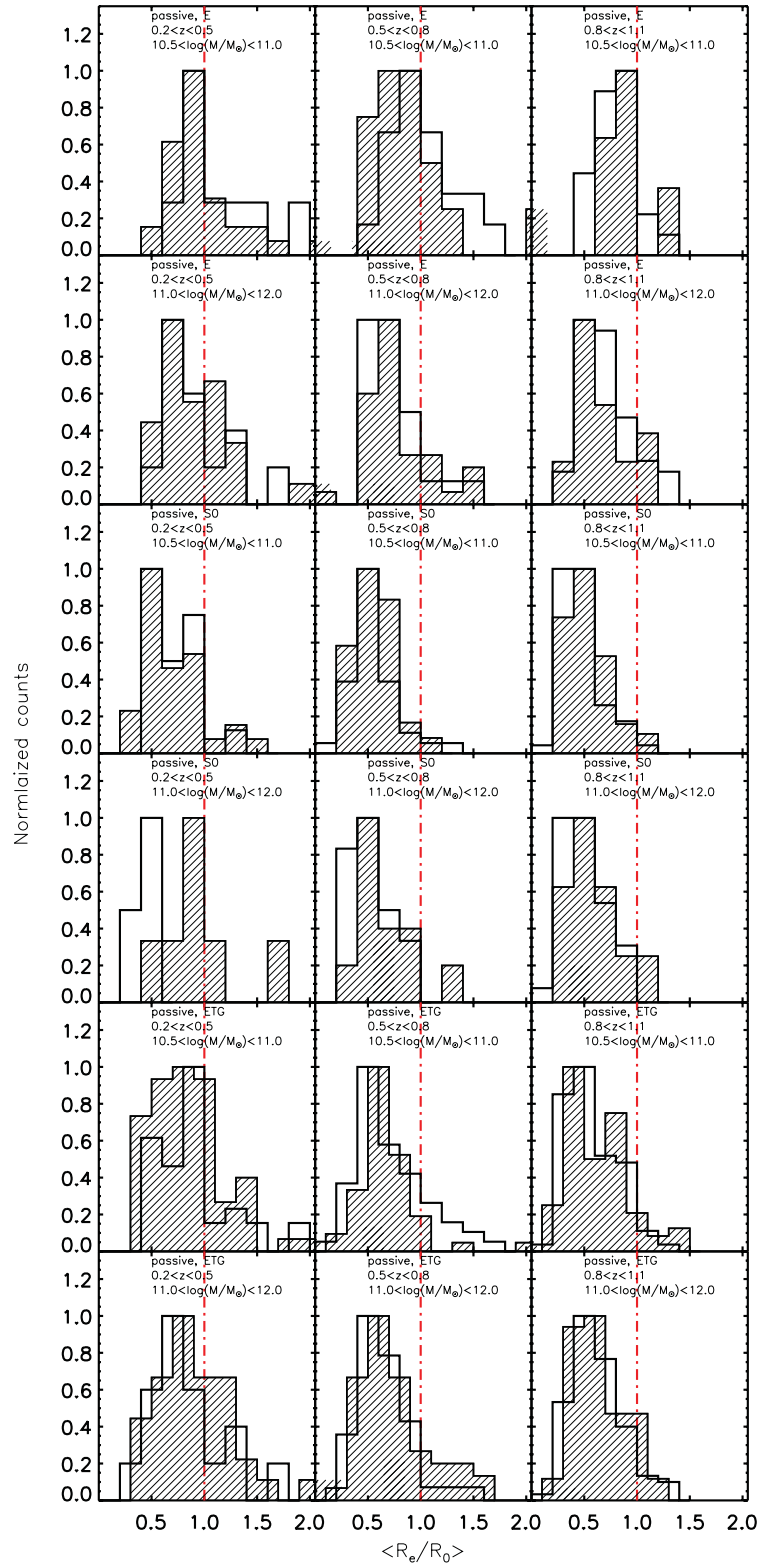
Figure 16. Size ratio distributions of group (filled histograms) and field galaxies (empty histograms) for different sample selections and different redshift and stellar mass ranges. The red dashed vertical line indicates a size ratio of 1. Each column shows a different redshift bin ($0.2 < z < 0.5$, $0.5 < z < 0.8$ and $0.8 < z < 1.1$ from left to right). Each row shows a different morphology and mass selection as explained in the text.

and minor mergers observed in COSMOS can explain ∼55 per cent of the size evolution of massive ($>10^{11}$ M$_\odot$) ETGs. If the progenitor bias of massive ETGs accounts for a factor of 1.25, this work can explain ∼75 per cent of the size evolution. We also

show, for completeness, in Fig. 18 the expected evolution taking into account this effect from that work (note however that the selection in terms of morphology and star formation is not exactly the same as the one used in this work). However, Whitaker et al.
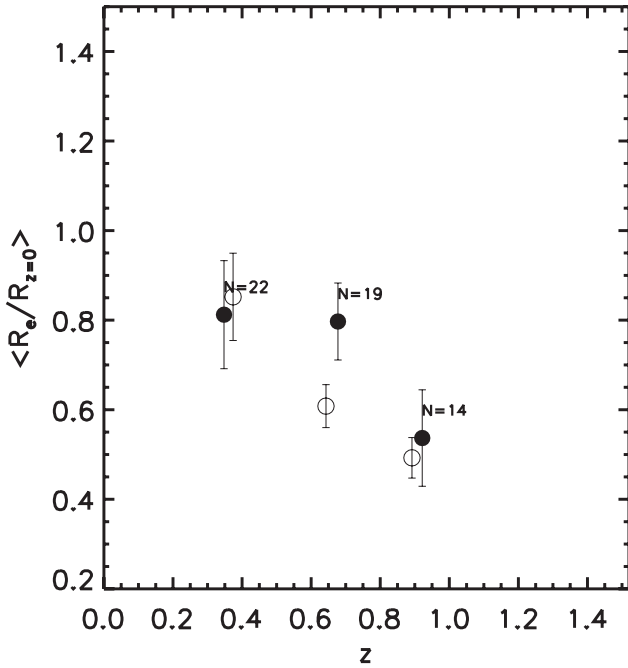
Figure 17. Size evolution of BCGs (filled circles) compared to satellite group members with $\log(M/M_\odot) > 11$ (empty circles). Numbers show the number of BCGs in each bin.

(2012) showed that the recently quenched galaxies at $1 < z < 2$ are not significantly larger than their older counterparts, suggesting that the effect of the so called progenitor bias is limited. Moreover, Fig. 11 also shows that the number densities (fractions) of massive ellipticals do not evolve significantly from $z \sim 1$, pointing again towards a reduced effect of newly formed galaxies.

There are also other possible tensions between merger models and current observations. A puffing-up of the external regions with no inner density variation as suggested by mergers (e.g. Naab et al. 2009) naturally produces an increase in the Sérsic index n of an

ideally light profile fitted to the projected density profile. In Fig. 19, we plot the median Sérsic index for massive elliptical galaxies. The median Sérsic index of the overall population does not evolve since $z \sim 1$. These results are in possible tension with this prediction [similar conclusions were found by Stott et al. (2011) for instance].

Another prediction of merger models is that galaxies residing at the centre of more massive haloes should, at fixed stellar mass, experience more mergers and thus be larger than their counterparts in less massive haloes, at least above $M_h > 5 \times 10^{12}\,M_\odot$, according to the analysis of Shankar et al. (2011). The latter, in fact, showed that BCGs should evolve much faster at $z < 2$, and also end up being larger than other galaxies of similar mass. We do not observe this trend.

4.1.2 Environmental dependences compared to model predictions

Concerning the dependence of galaxy sizes and their evolution on environment, we compare our observations to predictions from Shankar et al. (2011) in Fig. 20. We plot the mass-normalized radius as a function of halo mass for two redshift bins from COSMOS ($0.5 < z < 0.8$ and $0.8 < z < 1.0$), as well as for the local Universe from SDSS, for two mass ranges. All radii are shown in units of the mass-normalized radius measured in the field. Uncertainties in the observations have been calculated by bootstrapping 1000 times and recomputing the median of the distribution each time, as in all previously shown plots.

As discussed in Section 3 and summarized in Figs 15, 14 and 20, our COSMOS analysis does not show any significant dependence of median galaxy size on large-scale environment, e.g. galaxy sizes have similar medians in the field and in the groups. We observe the same in the SDSS sample, comparing measurements in galaxy groups from Yang et al. (2007) with the field.

The top panels of Fig. 20 compare observations to model predictions with no accounting for our sample size and observational uncertainties. In this case, the Shankar et al. (2011) model predicts that our most massive haloes should have mass-normalized radii of close to twice that of the field.
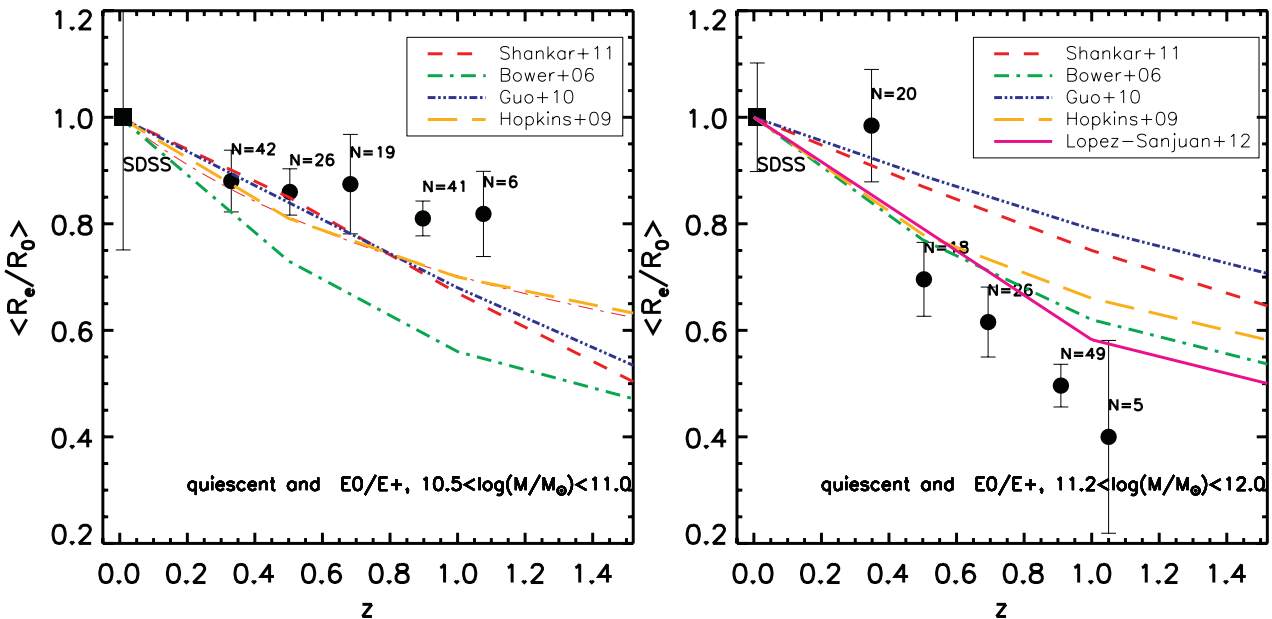
Figure 18. Size evolution of elliptical passive galaxies in two mass bins. Left-hand panel: $10.7 < \log(M/M_\odot) < 11$, right-hand panel: $\log(M/M_\odot) > 11.2$. Numbers indicate the number of objects in each redshift bin. Error bars are the scatter of the distributions. The different lines (see legend) show the prediction from different semi-analytic and empirical models (see the text for details).
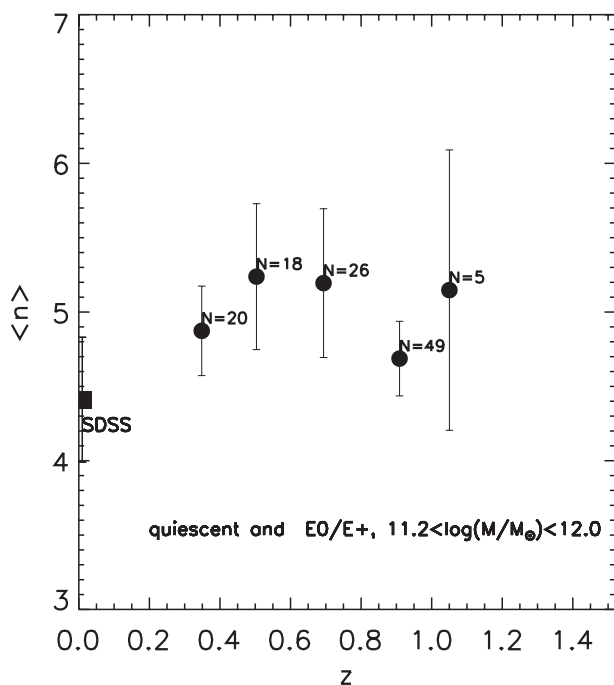
Figure 19. Median Sérsic index evolution for elliptical galaxies in the mass range $11.2 < \log(M/M_\odot) < 12$. The local point comes from the Sérsic decompositions of Simard et al. (2011) on visually classified ellipticals by Nair & Abraham (2010).

The middle and lower panels demonstrate that this strong difference is diluted when taking into account uncertainties intrinsic to our sample: the number of galaxies in each bin, the uncertainty due to photometric redshift estimation, and that on the estimate of the halo mass. In the middle panel, to properly compare observations with model predictions at each redshift and halo mass interval of interest, we perform 1000 Monte Carlo realizations in which we draw subsamples of galaxies from the Shankar et al. (2011) catalogue with numbers equal to those in the SDSS and COSMOS samples. Galaxies are selected to have $B/T > 0.5$ and to share the same stellar and halo mass intervals as in the observations, and sizes have been normalized to the local mass–size relation (Shankar et al. 2011). To each mock subsample we substitute 30 per cent (when comparing to COSMOS; George et al. 2011) and 20 per cent (when comparing to SDSS; Yang et al. 2007) of members with galaxies of the same stellar mass residing in the halo bin with the lowest mass in order to mimic contamination from the field (e.g. because of photometric redshift uncertainties). As expected, this tends to reduce the increase of mean size with halo mass by up to 20 per cent. For each Monte Carlo realization, we compute the mean and then extract, from the full distribution of means, the final mean and its 1σ error. In the lower panel, we add the further uncertainty due to halo mass estimation. We included in the simulations a Gaussian scatter of 0.3 dex width to reproduce the average uncertainties in the halo mass (Yang et al. 2007; Leauthaud et al. 2010).

When taking into account all these sources of uncertainties (lower panels of Fig. 20), the model predicts a much smaller difference in size between the most massive haloes and the field. Even if the trend observed in the upper panels still holds, when comparing our results obtained with COSMOS to the model, they are consistent at 1σ, i.e. the mass-normalized radius does not depend on environment. However, the larger SDSS sample shows that the model predicts sizes in groups to be about 1.5 times larger than those in the field, at

variance with the observations at more than 3σ. In future work, we will investigate if this result is specific to the particular model we consider (Shankar et al., in preparation) and/or to the observational data we have used (Huertas-Company et al., in press).

### 4.1.3 The size growth of lenticulars compared to model predictions

For what concerns lenticular galaxies (Fig. 21), model galaxies have been selected to have $0.4 < B/T < 0.7$. For this range of B/T, disc instabilities also play a non-negligible role in building bulges (see, e.g. Shankar et al. 2011, and references therein). Despite the significantly different procedures to grow bulges in the models, from mild instabilities (Guo et al. 2010) to violent ones (Bower et al. 2006), the result in the median size evolution is similar to the elliptical results. It is interesting to note that, analogously to what inferred with respect to more bulge dominated galaxies, hierarchical models are able to reproduce the trend in size evolution for lenticulars below $M_* < 10^{11}\,M_\odot$, but they tend to predict a shallower evolution above this mass.

4.2 Expansion

An alternative model for efficiently puffing up sizes of massive, ETGs, considers the galaxy expansion consequent to significant mass-loss via quasar and/or stellar winds (Fan et al. 2008, 2010; Damjanov et al. 2009). This model envisages that all massive ($M_* > 3 \times 10^{10}\,M_\odot$) ETGs forming at $z > 1$ went through a rapid expulsion of large amounts of mass, possibly caused by a powerful quasar wind, that caused the galaxy to expand. Numerical experiments in favour of this physical scenario have been performed by Ragone-Figueroa & Granato (2011), who showed that even in the presence of large amounts of DM, massive galaxies can significantly expand their sizes by a factor approximately proportional to the fraction of mass-loss. Fan et al. (2008) predict that most of the size evolution for the massive spheroidal galaxies should be delayed with respect to the peak of quasar activity by about 0.5–1 Gyr. The model also predicts a milder and possibly longer size evolution for ETGs with stellar mass below $M_* < 2 \times 10^{10}\,M_\odot$, for which the dominant energy input in the interstellar medium comes from supernovae explosions.

Clearly, the typical evolutionary time-scales to fully evolve a galaxy on to the local size–mass relation in the Fan et al. (2010) model are in general quite shorter than the cosmological ones required by a merger scenario. While a fast evolution in the size growth of massive ellipticals is supported by our data, their model predicts strong size evolution mainly at $z > 1$, while our data show strong size evolution also at $z < 1$, at least for massive ellipticals.

Fan et al. (2010) also point out that a fast size evolution necessarily should lead to the co-existence of large and compact quiescent galaxies at any redshift $z > 1$, and thus a large dispersion up to a factor of $<5-6$ in the size distribution at fixed stellar mass. The dispersion should then significantly reduce below $z < 1$, as most of the galaxies should be already evolved and their formation rate, which parallels the one of quasars peaking at $z = 2$ (Lapi et al. 2006), should progressively drop at late times (see their fig. 1). The dispersion in sizes for quiescent, massive ETGs that we measure from COSMOS seems instead to be rather contained, within a factor of 2 at fixed redshift and stellar mass. We also note, however, that our lower mass, quiescent ETG that have larger sizes might be, at least in part, composed of the population of high redshift, already evolved ETGs predicted by Lapi et al. (2006).
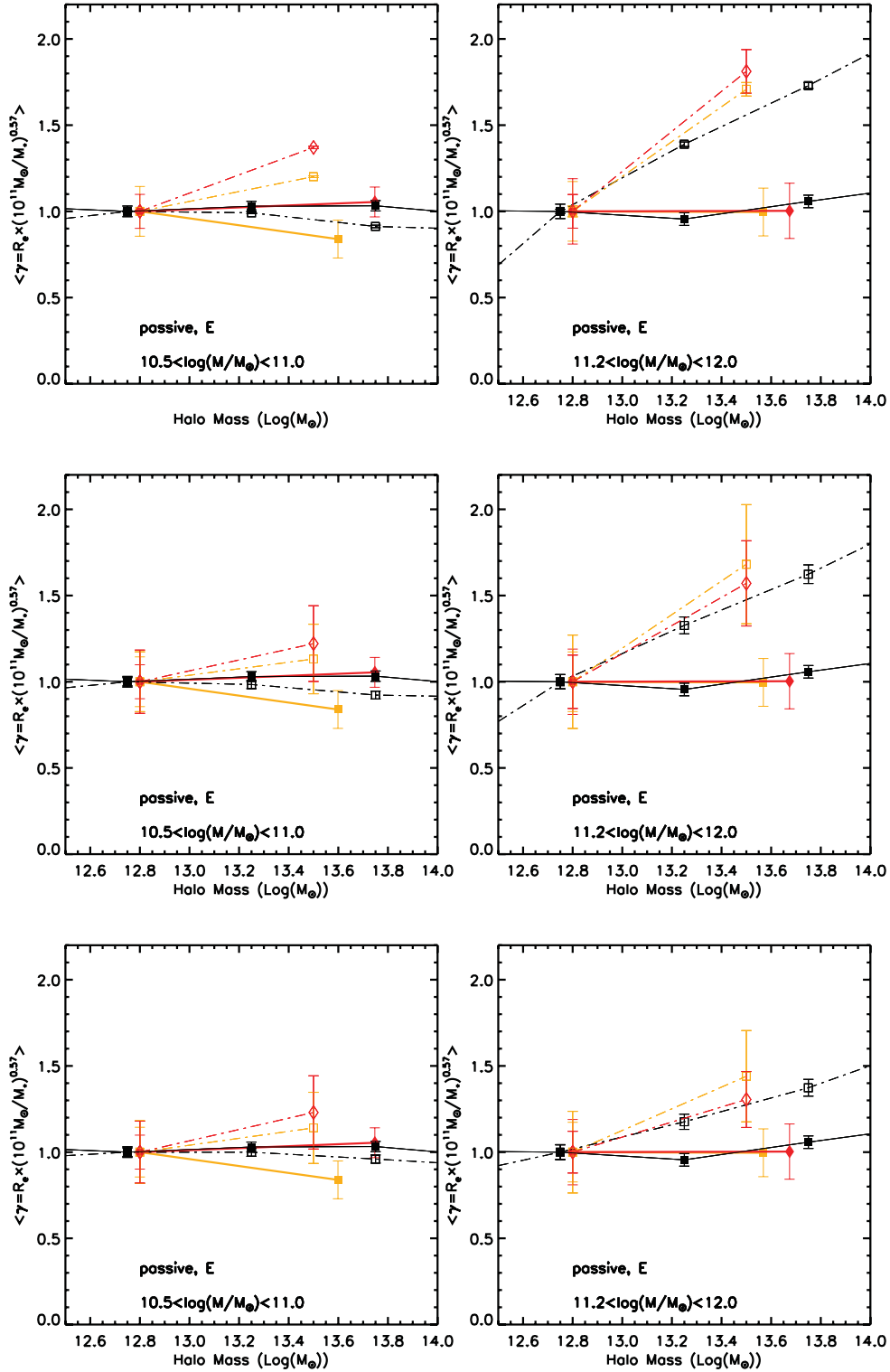
Figure 20. Size of elliptical galaxies as a function of halo mass for different redshift bins. The red diamonds are objects with $0.8 < z < 1.0$, the orange squares are $0.5 < z < 0.8$. The black, orange and red dash–dotted lines show the expected relation from Shankar et al. (2011) models at $z = 0$, 0.5 and 1, respectively. Values from models have been normalized so that, by definition, the field observed value at a halo mass of $\log(M_{\rm h}/M_{\odot}) = 12.8$–13 is equal to 1. The solid black line and the filled squares are the values measured from the SDSS and the group catalogue from Yang et al. (2007). The first row shows model prediction without errors, the second row shows results when the number of objects in models are selected to match the observations and $\sim$30 per cent field contaminations are included, finally the third row also includes a 30 per cent error in halo mass. Errors in models and observations are errors on the median values computed through bootstrapping (see the text for details).
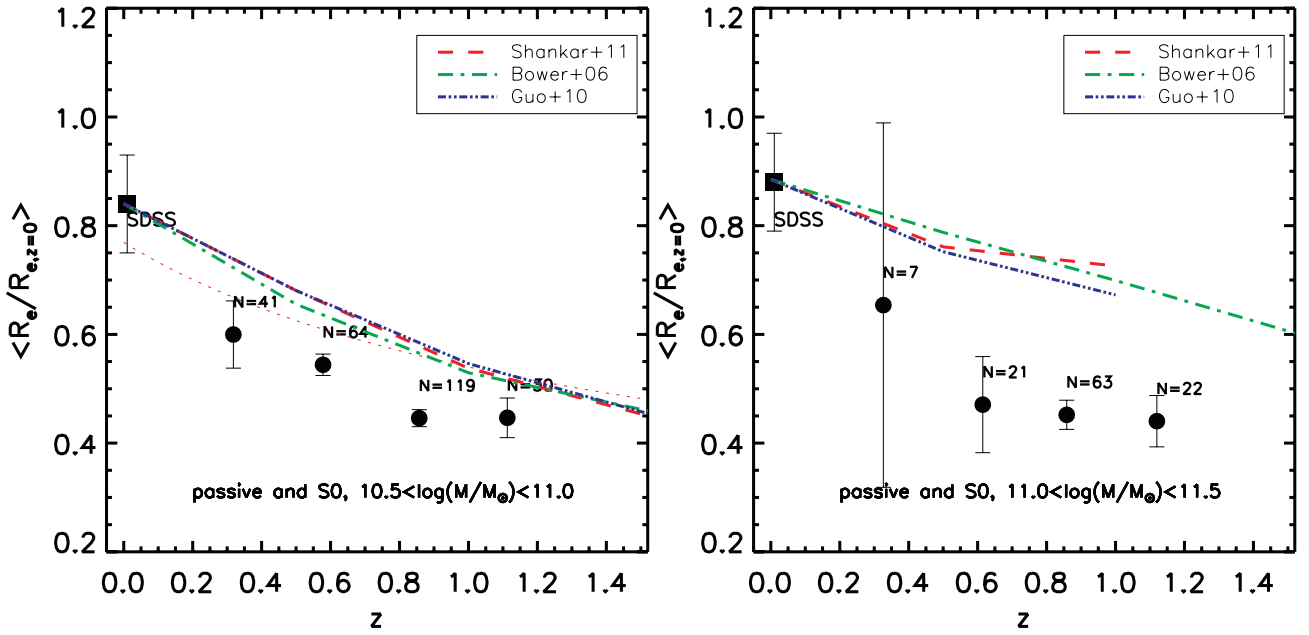
Figure 21. Size evolution of lenticular passive galaxies in two mass bins. Left-hand panel: $10.5 < \log(M/M_\odot) < 11$, right-hand panel: $\log(M/M_\odot) > 11.0$. Numbers indicate the number of objects in each redshift bin. Error bars are the scatter of the distributions. The red dotted line in the left-hand panel indicates the median evolution of star-forming discs in our sample divided by a factor of 1.3 to reach the same normalization. The other lines (see legend) show the prediction from different semi-analytic models (see the text for details).

The expansion model predicts that compact galaxies should be relatively young at the time of observation, being close to their formation epoch because the size evolution occurs only ~20 Myr after the expulsion via quasar feedback (Ragone-Figueroa & Granato 2011). This may be possibly at variance with the rather old ages that usually characterize massive ellipticals (see also Trujillo et al. 2011 for similar considerations based on observations).

On the other hand, Ragone-Figueroa & Granato (2011) also found in their numerical tests that the galaxy mass profiles should not change after the blow-out, if the mass-loss is contained to a factor of 2 or so. This might explain the nearly constancy with redshift of the Sérsic index in our sample. Also, being galaxy expansion an in situ physical mechanism, it should be largely independent of environment, as suggested by our data (Figs 15 and 20).

In summary, while merger models can explain most of the growth size $z \sim 1$, we find evidence that both proposed scenarios (mergers and mass-loss via quasar and/or stellar winds) suffer from some shortcomings with respect to our results and more advances in modelling are clearly needed to deeply understand how the two different scenarios shape the galaxy size evolution.

5 SUMMARY AND CONCLUSIONS

We have studied a sample of 3146 group galaxies and 3760 field galaxies from the COSMOS survey, and selected 298 group and 384 field galaxies as passive galaxies (based on their $M(NUV) - M(R)$ dust corrected rest-frame colour) with $\log(M/M_\odot) > 10.5$. We show, for the first time, how the mass–size relation and size growth depend on the detailed morphology of the quiescent population (mainly ellipticals and lenticulars) as well as on large-scale environment defined by the DM halo mass.

Our main results are as follows.

(i) A detailed morphological dissection of the passive population up to $z \sim 1$ reveals the following.

(a) About 80 per cent of all passive galaxies have an early-type morphology at all stellar masses and at all redshifts from $z \sim 1$. The remaining 20 per cent are essentially early-type spirals.

(b) ETGs are both ellipticals and S0s. At all redshifts up to $z \sim 1$, elliptical galaxies dominate the ETG population at masses $\log(M/M_\odot) > 11$–11.2. At $z < 0.5$, galaxies with masses $\log(M/M_\odot) < 11$ are around half ellipticals and half lenticular, while lenticulars dominate the low-mass fractions at $z > 0.5$. An important fraction of group and field low-mass passive galaxies in the redshift range $0.5 < z < 1$ are lenticular galaxies, e.g., which have a disc component (see also Bundy et al. 2010; Mei et al. 2012).

Therefore, studying the population of passive galaxies as a whole mixes different morphological populations which do not necessarily share the same evolutions.

(ii) When separating the ellipticals from the lenticulars, we show that *galaxy size evolution strongly depends on mass range and ETG morphology.*

(a) Massive ellipticals ($\log(M_*/M_\odot) > 11.2$) do experience a very strong size evolution from $z \sim 1$ to present ($r_e \propto (1 + z)^{-0.98 \pm 0.18}$). Even though the trend is somehow steeper than the one predicted by most of published semi-analytical models, minor dry mergers remain the most plausible explanation to the expansion. However, the Sérsic index of this population is not significantly evolving with time as expected from hierarchical models. We cannot exclude from our data that expansion via feedback might also play a role on the size evolution of this population.

(b) Less massive ellipticals ($10.5 < \log(M_*/M_\odot) < 11$) do not evolve much from $z \sim 1$ (from ~10 to ~30 per cent depending on which morphological classification we use). This behaviour is well reproduced by most of current semi-analytic models from which the size growth is mainly due to major and minor mergers.

c) The evolution observed in the lenticular population does not change significantly with stellar mass and they do show a size growth of 55 ± 10 per cent since $z = 1$.

(iii) Finally, we studied environmental effects on the size evolution by dividing our sample into field and group galaxies.

(a) We do not detect any significant evidence that the evolution of field and group galaxies ($13 < \log(M_{\mathrm{h}}/M_{\odot}) < 14.2$) with stellar masses $\log(M_*/M_{\odot}) > 11.2$ are different. This is observed both in the local Universe, when comparing SDSS groups from Yang et al. (2007) with field galaxies, and in our COSMOS group and field samples. This is also true for massive central ellipticals, where models clearly predict a major impact from mergers (Shankar et al. 2011).

This result is at variance with predictions from the standard hierarchical model (e.g. from Shankar et al. 2011), which predicts instead that the mass-normalized radius in our group mass range should be approximately two times larger than that in the field. When taking into account uncertainties due to our sample size, photometric redshift estimates and halo masses, this prediction remains, although the effect is reduced where our galaxy sample size is limited. Model predictions are consistent with our COSMOS results at 1σ, mainly because of the sample size. However, for our SDSS sample, the difference between the observed and predicted mass-normalized radii is at variance at $>3\sigma$. While the observations do not show any dependence of the mass-normalized radius with environment, Shankar et al. (2011) predict that galaxy mass-normalized radii over our group mass range should be ~1.5 larger than that in the field. In future work, we will investigate the dependence of this result on the specific model (Shankar et al., in preparation) and on the properties of SDSS sample (Huertas-Comany et al., in preparation) used here.

(b) BGGs and satellite galaxies of similar stellar mass ($\log(M_*/M_{\odot}) > 11$) evolve in a similar way. This is in disagreement with hierarchical models, which also predict a difference between centrals and satellites living in haloes with similar masses than our groups ($\log(M_*/M_{\odot}) \sim 13.4 - 13.6$). In fact, Shankar et al. (2011) have shown that galaxies residing at the centre of more massive haloes should, at fixed stellar mass, experience more mergers and thus be larger than their counterparts in less massive haloes.

Future work will involve a detailed discussion of environmental effects on models (Shankar et al., in preparation) as well as an extension to higher redshifts by studying the sizes of ETGs in distant clusters of galaxies (Delaye et al., in preparation).

ACKNOWLEDGMENTS

REFERENCES

Ascaso B., Aguerri J. A. L., Varela J., Cava A., Bettoni D., Moles M., D'Onofrio M., 2011, ApJ, 726, 69
Baillard A. et al., 2011, A&A, 532, A74
Barden M., Häußler B., Peng C. Y., McIntosh D. H., Guo Y., 2012, MNRAS, 422, 449
Bernardi M., 2009, MNRAS, 395, 1491
Bernardi M., Shankar F., Hyde J. B., Mei S., Marulli F., Sheth R. K., 2010, MNRAS, 404, 2087
Bertin E., Arnouts S., 1996, A&AS, 117, 393
Bezanson R., van Dokkum P. G., Tal T., Marchesini D., Kriek M., Franx M., Coppi P., 2009, ApJ, 697, 1290
Bluck A. F. L., Conselice C. J., Buitrago F., Gruetzbauch R., Hoyos C., Mortlock A., Bauer A. E., 2012, ApJ, 747, 34
Bower R. G., Benson A. J., Malbon R., Helly J. C., Frenk C. S., Baugh C. M., Cole S., Lacey C. G., 2006, MNRAS, 370, 645
Bruzual G., Charlot S., 2003, MNRAS, 344, 1000
Buitrago F., Trujillo I., Conselice C. J., Bouwens R. J., Dickinson M., Yan H., 2008, ApJ, 687, L61
Buitrago F., Trujillo I., Conselice C. J., Haeussler B., 2011, preprint (arXiv:1111.6993)
Bundy K. et al., 2006, ApJ, 651, 120
Bundy K. et al., 2010, ApJ, 719, 1969
Cameron E., 2011, PASA, 28, 128
Cassata P. et al., 2011, ApJ, 743, 96
Cimatti A., Nipoti C., Cassata P., 2012, MNRAS, L424
Cooper M. C. et al., 2011, ApJS, 193, 14
Cooper M. C. et al., 2012, MNRAS, 419, 3018
Daddi E. et al., 2005, ApJ, 626, 680
Damjanov I. et al., 2009, ApJ, 695, 101
Damjanov I. et al., 2011, ApJ, 739, L44
Fan L., Lapi A., De Zotti G., Danese L., 2008, ApJ, 689, L101
Fan L., Lapi A., Bressan A., Bernardi M., De Zotti G., Danese L., 2010, ApJ, 718, 1460
Finoguenov A. et al., 2007, ApJS, 172, 182
George M. R. et al., 2011, ApJ, 742, 125
Giodini S. et al., 2012, A&A, 538, A104
Gehrels N., 1986, ApJ, 303, 336
Grogin N. A. et al., 2011, ApJS, 197, 35
Guo Q., White S., Li C., Boylan-Kolchin M., 2010, MNRAS, 404, 1111
Häußler B. et al., 2007, ApJS, 172, 615
Hopkins P. F., Hernquist L., Cox T. J., Di Matteo T., Robertson B., Springel V., 2006, ApJS, 163, 1
Hopkins P. F., Bundy K., Murray N., Quataert E., Lauer T. R., Ma C.-P., 2009, MNRAS, 398, 898
Huertas-Company M., Rouan D., Tasca L., Soucail G., Le Fèvre O., 2008, A&A, 478, 971
Huertas-Company M., Foex G., Soucail G., Pelló R., 2009, A&A, 497, 743
Huertas-Company M., Aguerri J. A. L., Tresse L., Bolzonella M., Koekemoer A. M., Maier C., 2010, A&A, 515, A3
Huertas-Company M., Shankar F., Mei S., Bernardi M., Aguerri, J. A. L., Meert A., Vikram, V. 2012, ApjL (submitted)
Huertas-Company M., Aguerri J. A. L., Bernardi M., Mei S., Sánchez Almeida J., 2011, A&A, 525, A157
Ilbert O. et al., 2009, ApJ, 690, 1236
Kannappan S. J., Guie J. M., Baker A. J., 2009, AJ, 138, 579
Khochfar S., Silk J., 2006, ApJ, 648, L21
Koekemoer A. M. et al., 2007, ApJS, 172, 196
Koekemoer A. M. et al., 2011, ApJS, 197, 36
Lapi A., Shankar F., Mao J., Granato G. L., Silva L., De Zotti G., Danese L., 2006, ApJ, 650, 42
Leauthaud A. et al., 2010, ApJ, 709, 97
López-Sanjuan C. et al., 2011, A&A, 530, A20
López-Sanjuan C. et al., 2012, preprint (arXiv:1202.4674)
Maltby D. T. et al., 2010, MNRAS, 402, 282
Mancini C. et al., 2010, MNRAS, 401, 933
Martinez-Manso J. et al., 2011, ApJ, 738, L22
McLure R. J. et al., 2012, preprint (arXiv:1205.4058)
Mei S. et al., 2009, ApJ, 690, 42
Mei S. et al., 2012, ApJ, 754, 141
Meneux B. et al., 2009, A&A, 505, 463
Naab T., Johansson P. H., Ostriker J. P., 2009, ApJ, 699, L178
Nair P. B., Abraham R. G., 2010, ApJS, 186, 427
Newman A. B., Ellis R. S., Bundy K., Treu T., 2012, ApJ, 746, 162
Nipoti C., Treu T., Leauthaud A., Bundy K., Newman A. B., Auger M. W., 2012, MNRAS, 422, 1714
Oser L., Naab T., Ostriker J. P., Johansson P. H., 2012, ApJ, 744, 63
Papovich C. et al., 2012, ApJ, 750, 93
Patel S. G. et al., 2012, preprint (arXiv:1208.0341)
Peng C. Y., Ho L. C., Impey C. D., Rix H.-W., 2002, AJ, 124, 266
Postman M. et al., 2005, ApJ, 623, 721
Pozzetti L. et al., 2010, A&A, 523, A13

Ragone-Figueroa C., Granato G. L., 2011, MNRAS, 414, 3690

Raichoor A. et al., 2011, ApJ, 732, 12

Raichoor A. et al., 2012, ApJ, 745, 130

Rettura A. et al., 2010, ApJ, 709, 512

Rhodes J. D. et al., 2007, ApJS, 172, 203

Ryan R. E. Jr et al., 2012, ApJ , 749, 53

Saracco P., Longhetti M., Gargiulo A., 2011, MNRAS, 412, 2707

Sersic J. L., 1968, Atlas de Galaxias Australes, Cordoba, Argentina: Observatorio Astronomico

Shankar F. et al., 2011, preprint (arXiv:1105.6043)

Simard L., Mendel J. T., Patton D. R., Ellison S. L., McConnachie A. W., 2011, ApJS, 196, 11

Springel V. et al., 2005, Nat, 435, 629

Stott J. P., Collins C. A., Burke C., Hamilton-Morris V., Smith G. P., 2011, MNRAS, 414, 445

Tasca L. A. M. et al., 2009, A&A, 503, 379

Tiret O., Salucci P., Bernardi M., Maraston C., Pforr J., 2011, MNRAS, 411, 1435

Trujillo I. et al., 2006, ApJ, 650, 18

Trujillo I., Cenarro A. J., de Lorenzo-Cáceres A., Vazdekis A., de la Rosa I. G., Cava A., 2009, ApJ, 692, L118

Trujillo I., Ferreras I., de La Rosa I. G., 2011, MNRAS, 415, 3903

Trujillo I., Carrasco E. R., Ferré-Mateu A., 2012, ApJ, 751, 45

Valentinuzzi T. et al., 2010, ApJ, 712, 226

van de Sande J. et al., 2011, ApJ, 736, L9

van der Wel A., Holden B. P., Zirm A. W., Franx M., Rettura A., Illingworth G. D., Ford H. C., 2008, ApJ, 688, 48

van der Wel A. et al., 2011, ApJ, 730, 38

van Dokkum P. G. et al., 2008, ApJ, 677, L5

van Dokkum P. G. et al., 2011, ApJ, 743, L15

Weinmann S. M., Kauffmann G., van den Bosch F. C., Pasquali A., McIntosh D. H., Mo H., Yang X., Guo Y., 2009, MNRAS, 394, 1213

Whitaker K. E., Kriek M., van Dokkum P. G., Bezanson R., Brammer G., Franx M., Labbé I., 2012, ApJ, 745, 179

Williams R. J., Quadri R. F., Franx M., van Dokkum P., Toft S., Kriek M., Labbé I., et al., 2010, ApJ, 713, 738

Yang X., Mo H. J., van den Bosch F. C., Pasquali A., Li C., Barden M., 2007, ApJ, 671, 153

APPENDIX A: VISUAL MORPHOLOGICAL CLASSIFICATIONS

Some results presented in this paper are based on an automated morphological classification of galaxies at high redshift. Despite of the extensive tests performed to properly assess the accuracy of our classification, the separation of ellipticals from lenticulars might still remain a challenge. In this appendix, we want to make
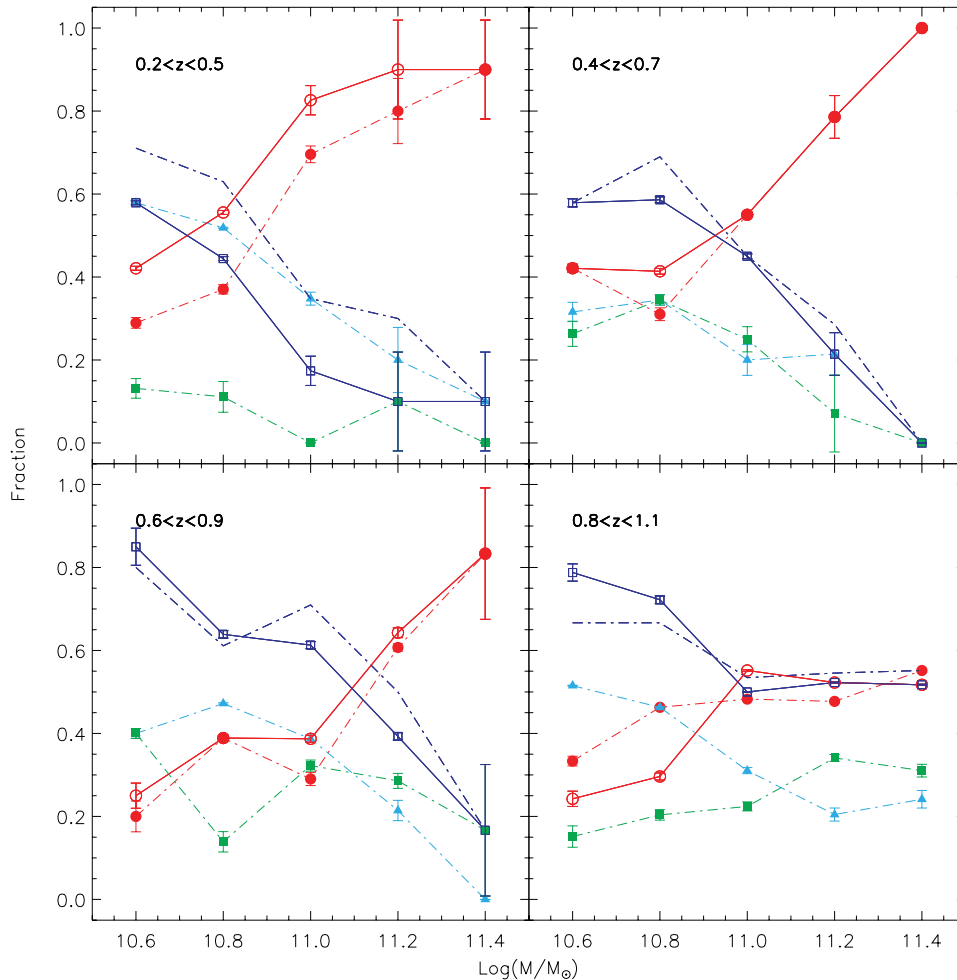
Figure A1. Morphological fractions of passive galaxies as a function of stellar mass and redshift using the visual morphological classifications by MHC (solid lines) and SM (dot–dashed lines). For MHC: the red solid lines are ellipticals and blue are galaxies with an observed disc component. For SM: the green lines are Sas, the cyan lines are S0s and the red lines are ellipticals. The dash–dotted blue line shows the fraction of galaxies with an observed disc component (S0s+Sas). The uncertainties are calculated following Gehrels (1986; see Section 3 for binomial statistics; see also Mei et al. 2009). These approximations apply even when ratios of different events are calculated from small numbers, and yield the lower and upper limits of a binomial distribution within the 84 per cent confidence limit, corresponding to 1σ.

sure that our results do not change while using an alternative classical visual classification. Two of us (SM and MHC) performed independent detailed visual classifications of all passive galaxies previously selected as early type by GALSVM (we assume that the separation between early and late is good enough). SM classified galaxies into three morphological classes (ellipticals, lenticulars and early spirals) while MHC followed a slightly different criterion and separated galaxies into two classes (disc and no disc). In Figs A2 and A3 we reproduce Figs 11, 12 and 13 respectively of the main text using the three morphological classifications (two visual and one automated). While there are some differences between the three estimates, the main trends discussed in the text do hold and the results are consistent within the error bars. This confirms that our morphological classification is robust and that the major results presented in the paper are not biased by the automated classification. Most of the differences between visual and automated classifica-
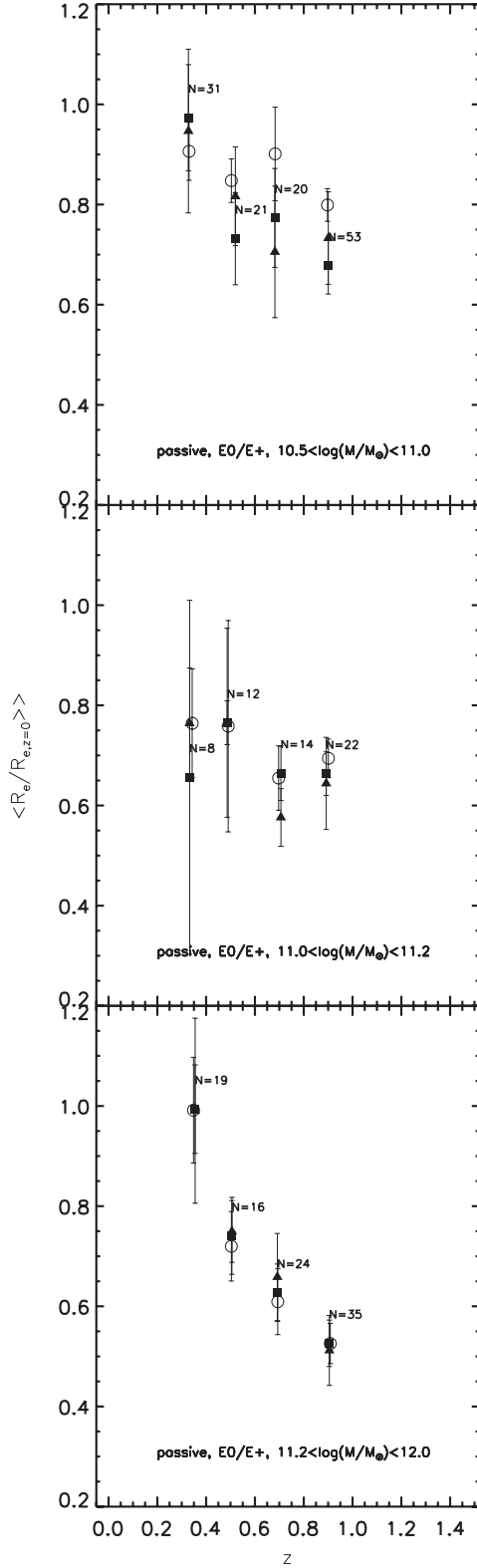
tions are seen in the low-mass elliptical population for which visual classifications show a steeper evolution than that estimated while using an automated classification. When the evolution of low-mass ellipticals is compared to their massive counterpart, it is still less steep as discussed in Section 3.2.1 and shown in Table A1.

APPENDIX B: ENVIRONMENT AND GALAXY SELECTION

In Fig. B1 we show the equivalent of Fig. 16 but only with galaxies having a probability $P_{MEM} > 0.8$ to be a group member and being at a distance $d < 0.5 \times R_{200}$ of the cluster centre. Our results do not change and remain basically the same as the ones shown in Table 2. The size distribution in mass and redshift bins does not depend on environment.
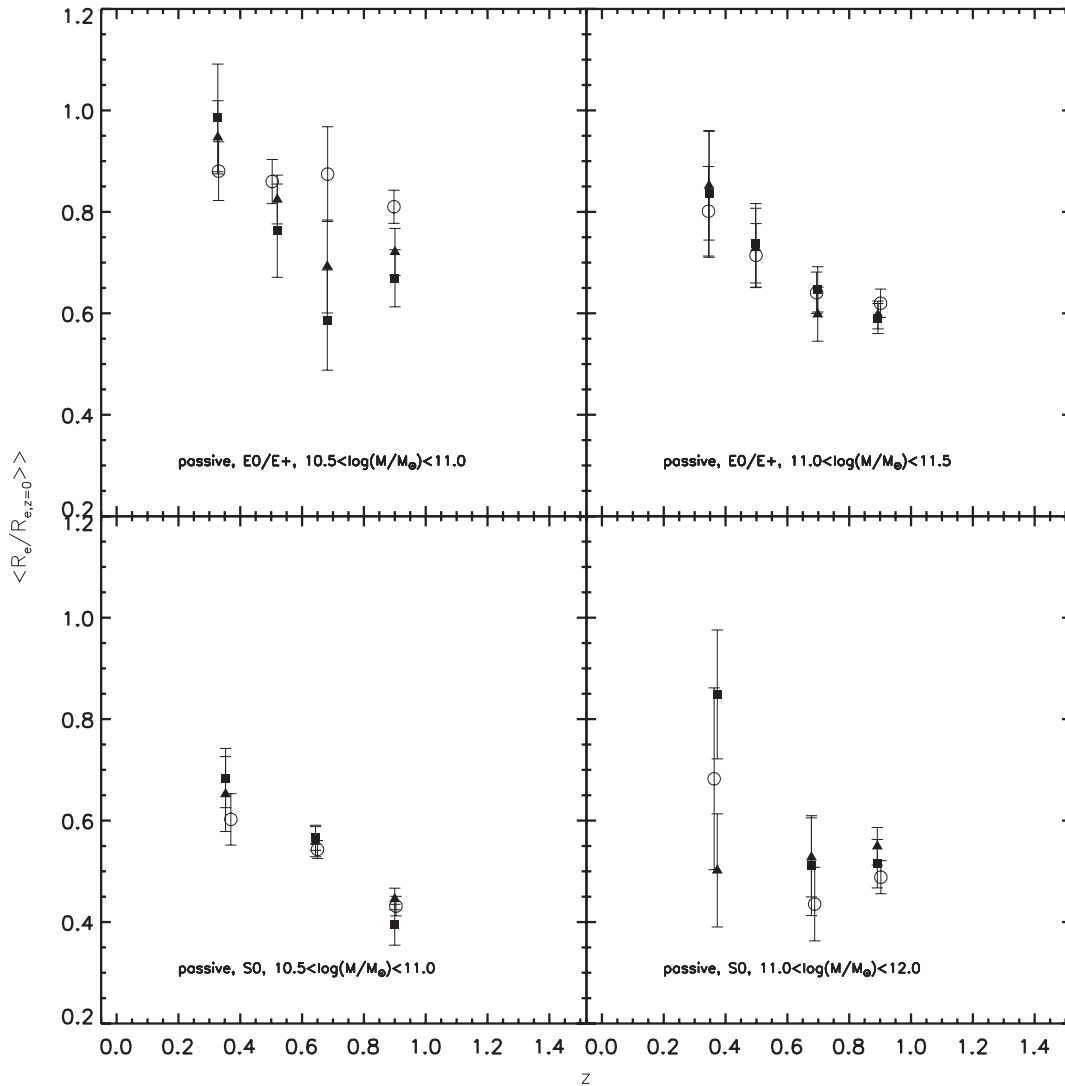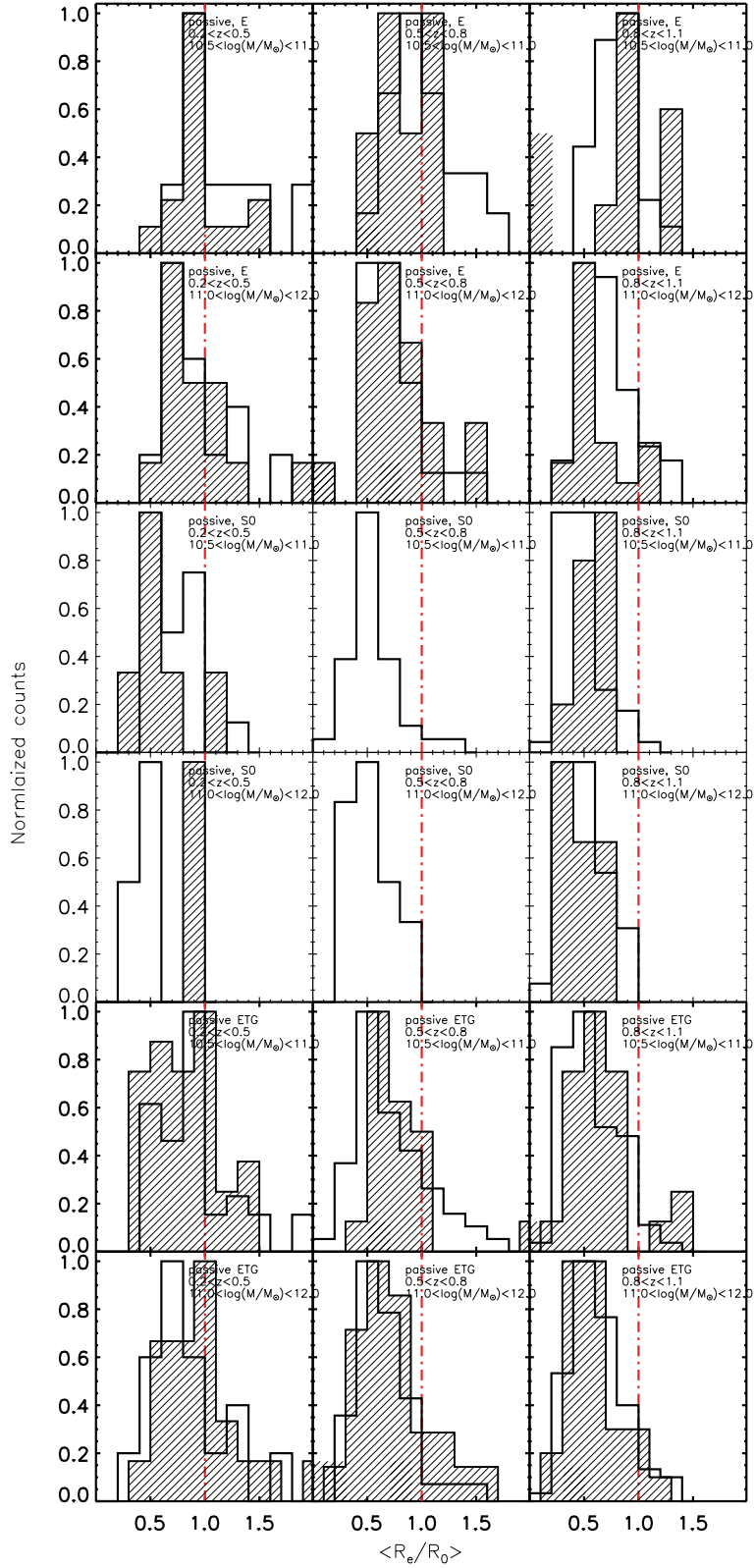

Figure A2. Size evolution of passive ellipticals (top row) and S0s (bottom row) in two different mass bins using three different morphological classifications (see the text for details). The empty circles show the automated classification from GALSVM, the squares are the visual classification from SM and the triangles are obtained with the visual classification of MHC.

Table A1. α values parametrizing the size evolution of ellipticals ($r_e \propto (1 + z)^{-\alpha}$) in three mass bins obtained using three different morphological classifications.

Stellar mass bin	Morphology	α
$10.5 < \log(M/M_\odot) < 11$	GALSVM	0.34 ± 0.17
	MHC	0.52 ± 0.23
	SM	0.59 ± 0.27
$11 < \log(M/M_\odot) < 11.2$	GALSVM	0.63 ± 0.21
	MHC	0.85 ± 0.22
	SM	0.61 ± 0.23
$11.2 < \log(M/M_\odot) < 12$	GALSVM	0.98 ± 0.21
	MHC	0.94 ± 0.21
	SM	0.95 ± 0.21

Figure A3. Size evolution of elliptical (left-hand column) passive galaxies in three mass bins using three different morphological classifications (see the text for details). The empty circles show the automated classification from GALSVM, the squares are the visual classification from SM and the triangles are obtained with the visual classification of MHC. Top row: $10.5 < \log(M/M_\odot) < 11$, middle row: $11.0 < \log(M/M_\odot) > 11.2$ and bottom row: $11.2 < \log(M/M_\odot) > 12$. Numbers indicate the number of objects in each redshift bin. Error bars are the scatter of the distributions.

Figure B1. Same as Fig. 16 but only for galaxies having a probability $P_{MEM} > 0.8$ to be a group member and being at a distance $d < 0.5 \times R_{200}$ of the cluster centre. Wherever only one histogram is shown it is because there are too few objects in that bin.

This paper has been typeset from a TEX/LATEX file prepared by the author.